



## Steady state and lean-rich cycling study of a three-way NO<sub>x</sub> storage catalyst: Experiments



Sotirios A. Malamis, Mengmeng Li, William S. Epling, Michael P. Harold\*

Department of Chemical and Biomolecular Engineering, Texas Center for Clean Engines, Emissions & Fuels, University of Houston, Houston, TX 77204, United States

### ARTICLE INFO

**Keywords:**

NO<sub>x</sub>  
Three-way catalyst  
Lean NO<sub>x</sub> trap  
Diesel  
Platinum

### ABSTRACT

The three-way NO<sub>x</sub> storage catalyst (TWNSC) combines components from a conventional three-way catalyst (TWC) and NO<sub>x</sub> storage and reduction (NSR) catalyst to improve NO<sub>x</sub> emissions while exploiting the higher fuel economy of lean-burn gasoline vehicles. The performance of a commercial monolithic TWNSC was studied to understand the NO<sub>x</sub> trapping and reduction performance over a range of conditions with emphasis on identifying conditions leading to optimal performance in terms of a standalone TWNSC or one coupled with a downstream selective catalytic reduction (SCR) device. Using H<sub>2</sub>, CO, and C<sub>3</sub>H<sub>6</sub> in various combinations, the impact of cycle timing (cycle time, rich duty fraction), reductant and O<sub>2</sub> feed concentrations, and feed temperature on NO<sub>x</sub> conversion and product (N<sub>2</sub>, NH<sub>3</sub>, N<sub>2</sub>O) selectivities was determined. Steady state experiments were conducted to assess catalyst activity and selectivity and to help interpret the phenomena observed during lean-rich switching. Cycling experiments reveal maxima in the NO<sub>x</sub> conversion and ammonia-to-NO<sub>x</sub> ratio (ANR) at distinct, intermediate cycle times. The existence of operating conditions giving these maxima depends on the reductant type, feed temperature, and O<sub>2</sub> feed concentration. For example, a large disparity in the lean/rich ratio (stoichiometric number) of the lean and rich feeds tends to lead to a NO<sub>x</sub> conversion maximum. Where possible, the data trends are interpreted in terms of known performance features of the TWC and NSR catalysts. The study findings provide guidance for optimizing the TWNSC formulation and operation strategy.

### 1. Introduction

Consumer demand for gasoline-powered vehicles spanning passenger cars to light-duty trucks and SUVs has generally increased over the past 6 years [1]. At the same time, vehicle manufacturers must respond proactively to the increasingly stringent emission and fuel economy standards through the development of more efficient and cleaner emitting vehicles [2]. This requirement has led to increased interest in lean-burn engines, which are typically more fuel efficient than their more conventional stoichiometric counterparts. Dual mode engine operation affords a combination of lean-burn and stoichiometric combustion with transitions between each depending on driving conditions and power needs [3]. Stoichiometric gasoline vehicles are equipped with three-way catalysts (TWCs) to simultaneously eliminate CO, HC<sub>s</sub>, and NO<sub>x</sub>. Fig. 1 shows the narrow air-to-fuel ratio window wherein TWCs are efficient in removing CO/hydrocarbons as well as NO<sub>x</sub>. Outside of this window, conversion of reductants (CO, HC<sub>s</sub>) is difficult under rich conditions and conversion of NO<sub>x</sub> is a challenge under lean conditions [4]. Fuel-lean operation results in excess (unreacted) O<sub>2</sub> in the exhaust gas. As a result, whereas the net oxidizing

exhaust enables the straightforward oxidation of partial combustion exhaust species CO and hydrocarbons (HC<sub>s</sub>), the catalytic reduction of NO<sub>x</sub> (NO + NO<sub>2</sub>) is more difficult [5,6]. Overall, TWCs are ineffective for the reduction of NO<sub>x</sub> in diesel or lean-burn gasoline vehicle exhaust.

Considerable progress in reducing NO<sub>x</sub> from diesel and lean burn gasoline vehicles has been made in recent years. Both the NO<sub>x</sub> storage and reduction (NSR) and selective catalytic reduction (SCR) technologies have been developed and commercialized [7]. NSR is a cyclic process wherein NO<sub>x</sub> is trapped during fuel-lean operating conditions and reduced to benign (N<sub>2</sub>), less harmful (CO<sub>2</sub>, N<sub>2</sub>O), or more useful species (NH<sub>3</sub>; see below) during a fuel-rich regeneration period [8]. Lean NO<sub>x</sub> trap (LNT) catalysts require a combination of oxidation, reduction, and NO<sub>x</sub> storage functionalities. Precious metals provide the first two functions, while oxides of alkaline earth metals provide the latter [9]. The basic LNT material contains BaO and Pt, with the former serving as the NO<sub>x</sub> storage material, and the latter providing catalytic sites for NO oxidation and NO<sub>x</sub> reduction [8,9]. Many previous studies have explored the NSR mechanism through which NO<sub>x</sub> is stored on the catalyst surface, i.e., the nitrite and nitrate routes [10]. Epling et al. provided evidence for two types of sites for NO<sub>x</sub> adsorption, namely

\* Corresponding author.

E-mail address: [mharold@uh.edu](mailto:mharold@uh.edu) (M.P. Harold).

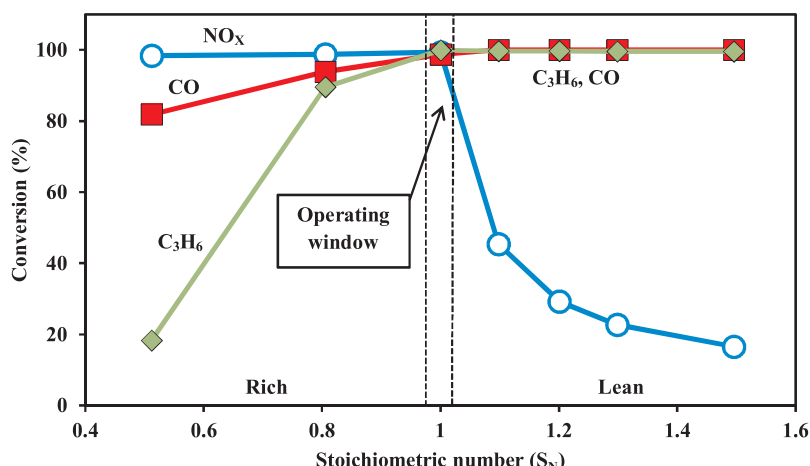


**Fig. 1.** TWC Performance Curve. Operating a TWC to the left or right of the operating window leads to significant performance loss. (The details of these data will be explained in the Results and Discussion section).

sites close to Pt that undergo the nitrite pathway, with subsequent oxidation to nitrates, and sites farther away where nitrates form via disproportionation [11]. Kumar et al. showed that the two populations of sites are a manifestation of stored NO<sub>x</sub> diffusion limitations [12].

During the subsequent rich phase or regeneration step the stored NO<sub>x</sub> is released and reduced, leading to the mixture of the aforementioned N-containing products: N<sub>2</sub>, N<sub>2</sub>O and NH<sub>3</sub>. Various studies detail the interaction between the precious metal and stored nitrates or nitrites on the surface, namely the reverse spillover process, in which “proximal” nitrates and nitrites decompose, leading to NO that is catalytically converted to N<sub>2</sub> on the Pt [9,13]. In addition to this chemistry, at high temperatures H<sub>2</sub>O can react with CO or HC to form H<sub>2</sub>, which results in higher selectivity to NH<sub>3</sub> [9,14,15]. Furthermore, the presence of H<sub>2</sub> on the Pt surface during this phase leads to H<sub>2</sub> dissociation that can reduce nearby NO species through a “forward spillover” process [16].

In contrast to NSR, selective catalytic reduction (SCR) requires the deliberate injection of NH<sub>3</sub> into or formation of NH<sub>3</sub> in the exhaust system; the latter is typically accomplished by the thermal conversion of aqueous urea [17]. Exhaust NO<sub>x</sub> combines with NH<sub>3</sub> and O<sub>2</sub> to form N<sub>2</sub> and H<sub>2</sub>O, mainly over zeolite catalysts via three main pathways: standard SCR (NH<sub>3</sub> + NO + O<sub>2</sub>); NO<sub>2</sub> SCR (NH<sub>3</sub> + NO<sub>2</sub>); and fast SCR (NH<sub>3</sub> + NO + NO<sub>2</sub>).

In recent years there has been increased interest in combining NSR and SCR technologies [18,19]. One such application involves the use of a LNT to generate NH<sub>3</sub> for a downstream SCR catalyst [19]. The main advantage of this approach is that an external source of NH<sub>3</sub> is not needed, while the main disadvantage is that periodic operation is required. One of the key metrics used to understand and to optimize SCR behavior is the ratio of NH<sub>3</sub> produced to NO<sub>x</sub> slippage from the upstream NSR catalyst (Ammonia-to-NO<sub>x</sub> ratio, ANR) [17,19–21].

In order to remove NO<sub>x</sub> from the exhaust gas and still operate the engine with a higher air to fuel ratio than the TWC, the concept of combining the TWC with NO<sub>x</sub> storage functionality was first proposed by Ikeda et Al. as the three-way NO<sub>x</sub> storage and reduction catalyst (TWNSC) [22]. While the TWNSC is generally applied to lean gasoline engine emission control, it serves a similar role as that of the sequence of the diesel oxidation catalyst (DOC) + LNT encountered in diesel emission control. Unlike the DOC + LNT, which operates with sustained lean-rich cycling, the TWNSC serves to trap NO<sub>x</sub> during the lean acceleration modes and to regenerate during coast/deceleration modes of engine operation. The challenge is to achieve a balance between the two catalyst functionalities while saving space and cost. As one might expect, there are many parameters involved in achieving or even optimizing this balance, such as the total cycle time, the fraction of the

cycle that the engine is in regeneration mode, etc. [9]. Performance metrics would certainly include conversion of NO<sub>x</sub>, CO, and HC, and the selectivity to N<sub>2</sub>, N<sub>2</sub>O, and NH<sub>3</sub>.

Recent experimental studies provide important insight about the modified TWC. The study by Theis et al. of a TWC + SCR system showed that all of the NH<sub>3</sub> was produced during the rich phase, implying the importance of finding the right balance between cycle time and conversion or selectivity [23]. DiGiulio et al. characterized different TWCs and their comparative abilities in generating NH<sub>3</sub> for use in a downstream SCR, a system referred to as passive-ammonia SCR [24]. In their work, four catalyst systems were examined, one of which was an NSR catalyst operating as a TWC. The study showed that the periodic operation expectedly generates NH<sub>3</sub> and the addition of a NO<sub>x</sub> storage component to a TWC lowers the required duration of the rich period while increasing the fuel economy. One of the main drawbacks is the decreased CO conversion at low catalyst temperatures; an effect that must be addressed in future studies [24].

The objective of this study is to systematically evaluate the performance of a commercial TWNSC under a range of cycling protocols. Specific attention is placed on the impacts of operating parameters on conversion and product distribution. The data are interpreted in terms of the anticipated application, be it a standalone unit intended to maximize the NO<sub>x</sub> conversion and N<sub>2</sub> selectivity or a TWNSC + SCR tandem unit in which the intent is to shift up to half of the NO<sub>x</sub> conversion to the downstream SCR. Conditions are identified that lead to best performance for each application. Where possible, the performance trends are interpreted from the standpoint of known TWC and NSR features. It is important to note that the TWNSC is meant to operate once the vehicle has warmed up to allow sufficient activity of the emission catalyst. In principle, the TWNSC could be modified to enable low temperature HC and NO<sub>x</sub> trapping. However, this effect was not a focus of the current study and thus low temperature data are not discussed.

## 2. Experimental

The commercial TWNSC used in this work was received from Fiat Chrysler Automobiles LLC. (FCA). The commercially supplied catalyst is a mixed catalyst containing precious group metals (PGM) comprising a mixture of TWC and LNT components such as barium oxide (for NO<sub>x</sub> storage), ceria (for oxygen storage), and alumina (binder). Table 1 provides the ICP-measured mass percentages of the oxide components (Ba, Ce, Al, La, and Zr). The precious group metal mass percentage was ~1.2 wt.% in a Pd:Pt:Rh ratio of 73:26:1. Samples were cut from a monolith “brick” to ~1 cm in diameter and 1.8 cm long. CO

**Table 1**

Mass percentages of the washcoat oxide components measured by ICP.

Element	Al	Ba	Ce	La	Pt + Pd + Rh	Zr
wt.%	19.30%	4.70%	9.96%	1.22%	1.16%	8.92%

chemisorption using a Micromeritics apparatus gave a PGM metal dispersion of ~40% for a fresh sample, before degreening. Because the ratio of Pd:Pt:Rh in the sample is known, an average value for the stoichiometry factor was determined in order to calculate the dispersion, which in this case is 1.0. One sample was used for all the catalyst performance experiments conducted in this work, which was degreened at 700 °C for 4 h in 10% H<sub>2</sub>O and 10% CO<sub>2</sub> with a balance of Ar. The sample was then wrapped in ceramic paper and placed in a horizontal-flow quartz tube reactor. The total flow rate was kept constant at 3000 sccm (standard cm<sup>3</sup>/min), which corresponds to a gas hourly space velocity at standard conditions of 99,000 h<sup>-1</sup>. Inlet and outlet lines were maintained at 180 °C to prevent condensation. Effluent concentrations were measured using a Thermo Scientific FT-IR (6700 Nicolet). Three type-K thermocouples (Omega Engineering) were used to monitor the temperatures within the system. One was placed 0.5 cm upstream of the catalyst (T<sub>feed</sub>); the second was placed in the radial and axial center of the catalyst (T<sub>cat</sub>); and the third was placed 0.5 cm downstream (T<sub>out</sub>). T<sub>feed</sub> and T<sub>cat</sub> were used as the reference temperatures for the experiments in this work.

For the steady state experiments, the catalyst was first pretreated with 5% O<sub>2</sub>, 10% CO<sub>2</sub>, and 7% H<sub>2</sub>O at 500 °C for 20 min. After the pretreatment, the reactor was purged for 10 min with Ar, and was cooled to the desired feed temperature during which time a steady flow of feed gases was established through the bypass. Once the reactor temperature was stable, the flow was switched from the bypass to the reactor, and the effluent concentrations were monitored until steady concentrations ( $\pm 2\%$ ) were obtained for at least 10 min. The desired feed temperature was achieved by adjustment of the furnace temperature.

NO<sub>x</sub> storage experiments were conducted in the same quartz tube reactor. First, the catalyst was pretreated in a feed of 2% H<sub>2</sub> at the feed temperature for 30 min, after which the catalyst was purged under argon for 10 min. During adsorption, a feed containing 500 ppm NO and 5% O<sub>2</sub> was introduced to the catalyst until the output concentration reached steady state (i.e. saturation). The NO/O<sub>2</sub> mixture was then turned off and the catalyst was held at the adsorption temperature until the outlet concentration of NO<sub>x</sub> reached zero, eliminating any weakly adsorbed NO<sub>x</sub> from the surface. Then the catalyst underwent a temperature-programmed desorption under Ar at a rate of 10 °C/min up to 600 °C. This procedure was repeated for a variety of feed temperatures ranging from 130 °C to 415 °C.

In this work, the stoichiometric number is used to characterize the feed composition:

$$S_N = \frac{2C_{O_2} + C_{NO}}{C_{CO} + C_{H_2} + 9C_{C_3H_6}} \quad (1)$$

S<sub>N</sub> measures the deviation of the catalyst environment from a stoichiometric neutral feed (S<sub>N</sub> = 1). Unless otherwise specified, the feed composition consisted of 1% CO, 3300 ppm H<sub>2</sub>, 500 ppm NO, 10% CO<sub>2</sub>, 7% H<sub>2</sub>O, and a variable concentration of O<sub>2</sub> to achieve a certain S<sub>N</sub>. When propylene was used its concentration was 1000 ppm. The balance of all mixtures was Ar in order to maintain a constant total feed flow-rate and space velocity.

For the cycling experiments, the same pretreatment was used, followed by a 10 min Ar purge. Instead of establishing a steady flow through the bypass, a steady cycling profile through the bypass was obtained. A pseudo steady state was defined by an unchanging effluent temporal profile for at least 5 cycles. Once the feed was established and the reactor temperature stabilized, the flow was switched to the reactor

tube and effluent concentrations were measured until 10 repeatable cycles were obtained. The feed system enables precise control of the rich and lean feeds to as short as a 1 s duration. In this study, typical total cycle times,  $\tau_T$ , were in the range of 20–60 s with rich duty fractions,  $d_r$ , between 0.05 and 0.7, with the following definitions:

$$\tau_T = \tau_r + \tau_l \quad (2a)$$

$$d_r = \frac{\tau_r}{\tau_T} \quad (2b)$$

Details of more complex cycling experiments are described later in the Results and Discussion section of this work.

Several performance metrics were defined and calculated, including reactant conversion, selectivity, and yield. The cyclic values were time integrated over at least 5 cycles, yielding a cycle-averaged value. The cycle-averaged NO<sub>x</sub> conversion is defined as:

$$X_{NO_x} = \frac{\int C_{NO_{x,in}} - \int C_{NO_{x,out}}}{\int C_{NO_{x,in}}} \quad (3)$$

with the NO<sub>x</sub> concentration the sum of NO and NO<sub>2</sub>. The cycle-averaged CO conversion is similarly defined as:

$$X_{CO} = \frac{\int C_{CO_{in}} - \int C_{CO_{out}}}{\int C_{CO_{in}}} \quad (4)$$

A similar equation was used to calculate the conversion of C<sub>3</sub>H<sub>6</sub>. The corresponding steady state quantities were obtained using standard definitions. The cycle-averaged selectivity of the N-containing product is given by:

$$S_{N_{species}} = \frac{\alpha \int C_{N-species,out}}{\int C_{NO_x reacted}} \quad (5)$$

where  $\alpha$  represents the molar coefficient of the species ( $\alpha = 1$  for NO, NO<sub>2</sub> and NH<sub>3</sub>;  $\alpha = 2$  for N<sub>2</sub>O). The N<sub>2</sub> selectivity was calculated by difference of the other species selectivities. The NH<sub>3</sub> yield is defined by:

$$Y_{NH_3} = \frac{\int C_{NH_3,out}}{\int C_{NO_x,in}} \quad (6)$$

In addition to conversion and selectivity, the cycle-averaged temperature was determined using a similar time-integrated method. Finally, the ratio of ammonia produced to NO<sub>x</sub> slip (ANR) is defined by:

$$ANR = \frac{\int C_{NH_3,out}}{\int C_{NO_x,out}} \quad (7)$$

The lean NO<sub>x</sub> storage efficiency,  $\eta_l$ , is the fraction of NO<sub>x</sub> stored during the lean phase of duration  $\tau_l$ :

$$\eta_l = \frac{C_{NO_{in}} * \tau_l - \int C_{NO_{x,out}} d\tau_l}{C_{NO_{in}} * \tau_l} * 100 \quad (8)$$

### 3. Results and discussion

#### 3.1. Steady state catalyst performance

A series of steady state experiments was used to characterize the TWNSC activity and performance over a range of feed temperatures and compositions spanning lean to rich as described above in the Experimental section.

The steady state NH<sub>3</sub>, CO, NO<sub>x</sub>, and N<sub>2</sub>O effluent concentrations under various lean or rich feed conditions at a fixed feed temperature of 270 °C are shown in Fig. 2. The figure also reports the mid-core temperature rise, measured as the difference between mid-catalyst temperature and feed temperature, T<sub>cat</sub> – T<sub>feed</sub>. The inset shows an expanded view of the 0.85 < S<sub>N</sub> < 1.15 range, and also includes concentrations of individual NO<sub>x</sub> components NO and NO<sub>2</sub>. The stoichiometric condition (S<sub>N</sub> = 1) is the demarcation between the lean and

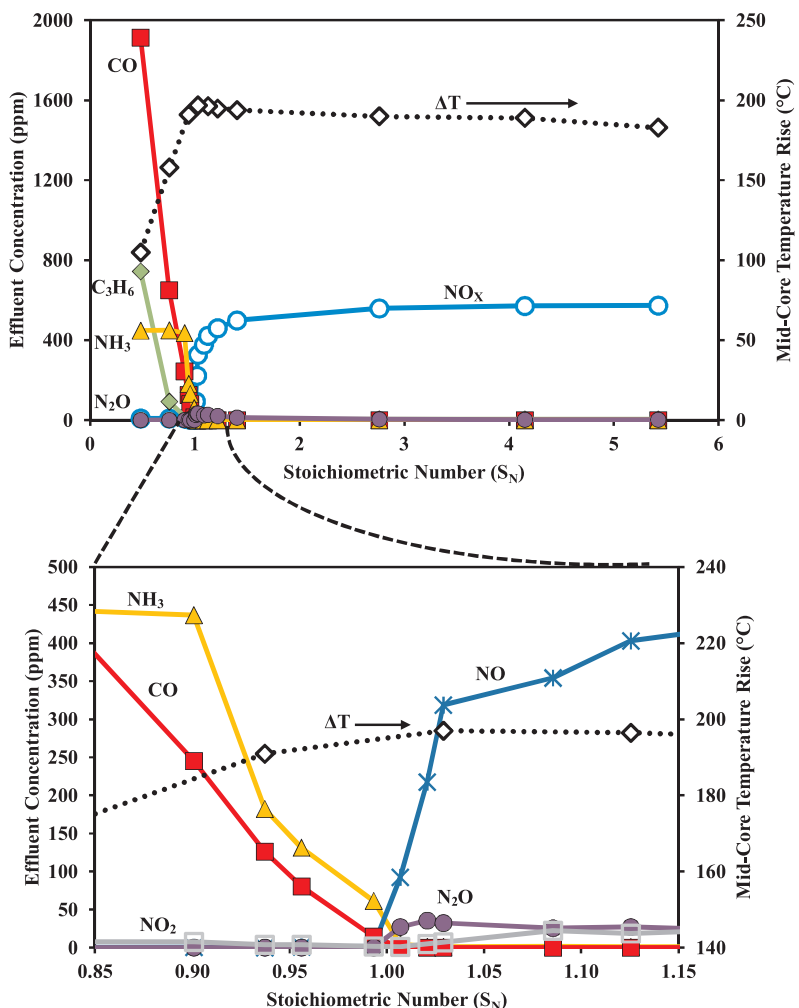


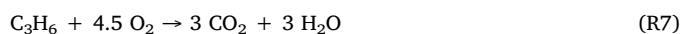
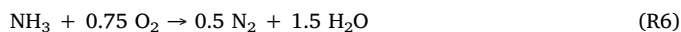
**Fig. 2.** Steady state effluent concentrations of NH<sub>3</sub>, CO, C<sub>3</sub>H<sub>6</sub>, NO<sub>x</sub> (incl. NO and NO<sub>2</sub>), and N<sub>2</sub>O (ppm) and catalyst temperature rise (°C) vs. stoichiometric number (S<sub>N</sub>) varying from lean to rich. T<sub>feed</sub> = 270 °C. Inlet concentrations of CO = 1%, NO = 500 ppm, C<sub>3</sub>H<sub>6</sub> = 1000 ppm, H<sub>2</sub> = 3300 ppm, H<sub>2</sub>O = 7%, CO<sub>2</sub> = 10%, varied O<sub>2</sub>.

rich feeds. At S<sub>N</sub> = 1 the reacting species concentrations approach zero, as expected.

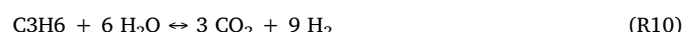
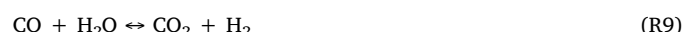
To the left of the neutral feed (Fig. 2) is the rich regime (S<sub>N</sub> < 1). As S<sub>N</sub> decreases from unity, the NH<sub>3</sub> concentration increases, the CO and C<sub>3</sub>H<sub>6</sub> concentrations increase (conversions decrease), and the NO<sub>x</sub> concentration approaches zero (complete NO<sub>x</sub> conversion). In an O<sub>2</sub> deficient condition the NO<sub>x</sub> is reduced to either N<sub>2</sub> or NH<sub>3</sub> with negligible production of N<sub>2</sub>O. The increasing levels of CO and C<sub>3</sub>H<sub>6</sub> with decreasing S<sub>N</sub> result in a shift to NH<sub>3</sub> as the main N-containing product. Global chemical reactions that occur under rich conditions include NO reduction by the reductants:



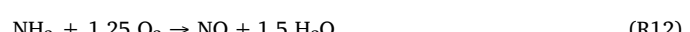
Under rich conditions both complete and partial oxidation reactions may occur:



Additionally, reactions involving H<sub>2</sub>O as a reactant include water gas shift and reforming:



To the right of the stoichiometric condition is the lean regime (S<sub>N</sub> > 1). The global reactions occurring under the stoichiometric excess are expectedly oxidation of the various species, including the previously identified total oxidation reactions (R4, R5, R6, and R7). Other oxidation reactions that can occur, include NH<sub>3</sub> oxidation to N<sub>2</sub>O and NO:



and NO oxidation to NO<sub>2</sub>:



The distribution of nitrogen oxides depends on the temperature and O<sub>2</sub> concentration, among other factors [21]. For this set of conditions, NO oxidation to NO<sub>2</sub> in the range of 1.0 < S<sub>N</sub> < 1.5 is minimal. The low NO<sub>2</sub> concentration is in part a result of its reactivity as an oxidant. Reaction may also occur between NH<sub>3</sub> and NO especially near the

stoichiometric point. As  $S_N$  increases from unity, very little  $\text{NH}_3$ ,  $\text{CO}$ , and  $\text{C}_3\text{H}_6$  are detected due to their respective oxidations, while a low but nonzero  $\text{N}_2\text{O}$  concentration is observed, as well as a shallow  $\text{N}_2\text{O}$  maximum at  $S_N \sim 1.02$ , before decreasing towards zero for  $S_N > 1.5$ .  $\text{NO}_x$  concentrations increase sharply with increasing  $S_N$ , approaching the feed value of 500 ppm by  $S_N \sim 2$ . The inset reveals that in a slight excess of  $\text{O}_2$  ( $S_N \sim 1.01$ ) all of the reductants are oxidized, as expected. The negligible but non-zero  $\text{N}_2\text{O}$  level for higher  $S_N$  is attributed to the presence of  $\text{NO}$  and  $\text{O}_2$  in the gas phase [25]. Under these slightly lean steady state conditions, the precious metal sites are occupied by an admixture of  $\text{O}$ ,  $\text{NO}$  and  $\text{N}$  species.  $\text{N}_2\text{O}$  can form through the following reaction [26]:

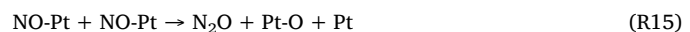


The  $\text{N}_2\text{O}$  maximum reflects adsorbed oxygen inhibition of  $\text{NO}$  sorption and reaction. At sufficiently large  $S_N$  the inhibition is sufficient so as to prevent  $\text{N}_2\text{O}$  formation.

The catalyst temperature rise reaches a maximum of  $\sim 200^\circ\text{C}$  near  $S_N = 1$ . The maximum is attributed to the complete conversion of the reductants that results in the highest exotherm. With the temperature rise as a measure of the aggregate conversions of the reactants, it follows that full conversion of all species leads to the highest temperature rise. The slight decrease with increasing  $S_N$  beyond 1 is due to the non-adiabatic nature of the reactor. With increasing  $S_N$ , the oxidation reactions occur at higher rates, and thus became more localized towards the upstream portion of the catalyst. As the reactions occur more in the upstream portion, some heat loss can occur downstream.

Fig. 3 shows the conversions and selectivities of the reacting and product species over a range of feed temperatures for a slightly lean, almost stoichiometric feed ( $S_N = 1.01$ ). The  $\text{NO}_x$ ,  $\text{C}_3\text{H}_6$ , and  $\text{CO}$  conversions are shown in Fig. 3a, while the selectivities to  $\text{N}_2\text{O}$ ,  $\text{NH}_3$ , and  $\text{N}_2$  (by difference) are shown in Fig. 3b. As the feed temperature

increases from  $\sim 150$  to  $200^\circ\text{C}$ , the  $\text{CO}$  and  $\text{C}_3\text{H}_6$  conversions sharply increase to 100%. In contrast, the  $\text{NO}_x$  conversion reaches a 60% maximum at  $\sim 275^\circ\text{C}$  before decreasing to  $\sim 35\%$  at  $500^\circ\text{C}$ . The  $\text{NO}_x$  conversion maximum is attributed to the competing effects of adsorption, desorption, and reaction. At low temperature,  $\text{CO}$  and  $\text{NO}$  are not converted due to self-inhibition [27]. As the temperature increases, surface reactions commence, including  $\text{CO}$  and  $\text{C}_3\text{H}_6$  oxidation, as well as  $\text{NO}_x$  conversion to  $\text{N}_2\text{O}$  and  $\text{N}_2$ . The abrupt increase in conversion of  $\text{CO}$  and  $\text{C}_3\text{H}_6$  is indicative of a reduction in  $\text{CO}$  coverage due to  $\text{CO}$  desorption, freeing up sites for oxidation. At sufficiently high temperature an increased rate of  $\text{NO}$  desorption leads to a decline in  $\text{NO}_x$  conversion. The decreasing  $\text{N}_2\text{O}$  selectivity (Fig. 3b) is due in part to a declining availability of  $\text{NO}$  due to the increasing  $\text{NO}$  desorption rate. That  $\text{N}_2\text{O}$  is highest at low temperature is a result of the lower rate of  $\text{N}-\text{O}$  bond scission, making  $\text{NO}$  available to react through  $\text{N}-\text{NO}$  (R14) or  $\text{NO}-\text{NO}$  coupling [28]:



$\text{N}_2\text{O}$  formation sharply decreases at higher temperatures due to the increased selectivity to  $\text{N}_2$ , a result of an increased rate of  $\text{N}-\text{O}$  bond scission at higher temperatures, minimizing the presence of  $\text{NO}$  available for  $\text{N}-\text{NO}$  coupling, and yielding  $\text{N}-\text{N}$  coupling instead.

Finally,  $\text{NH}_3$  formation is favored under rich conditions, which for  $S_N = 1.01$  (slightly lean) is negligible [29]. The observed small but nonzero  $\text{NH}_3$  selectivity at  $150^\circ\text{C}$  is attributed to low temperature formation of  $\text{NH}_3$  via  $\text{H}_2$ , even though the feed is slightly lean. It was previously shown that  $\text{H}_2$  reacts readily with  $\text{NO}$  to form a mixture of  $\text{N}_2\text{O}$ ,  $\text{N}_2$ , and  $\text{NH}_3$  on Pt at low temperature and anaerobic conditions [30]. In the presence of a slight excess of  $\text{O}_2$  there is competition between  $\text{O}_2$  and  $\text{NO}$  to oxidize  $\text{H}_2$ , leading to the negligible but nonzero formation of  $\text{NH}_3$ . That is,  $\text{H}_2$  oxidation by  $\text{O}_2$  is apparently not fast enough at low temperatures, allowing for  $\text{NO}$  reduction by  $\text{H}_2$ .

### 3.2. $\text{NO}_x$ storage evaluation

In order to evaluate the ability for the TWNSC to store  $\text{NO}_x$  during the lean phase, a series of experiments was conducted at a variety of feed temperatures in which a feed of 500 ppm  $\text{NO}$  and 2%  $\text{O}_2$  was fed over the catalyst. The results of this experiment are shown in Fig. 4, which plots the average amount of total  $\text{NO}_x$  adsorbed and desorbed vs feed temperature. Because the adsorption experiment was conducted until the catalyst reached saturation of  $\text{NO}_x$ , the values in Fig. 4 represent the total  $\text{NO}_x$  storage capacity of the TWNSC at the given feed temperature. The error between the calculated amount of stored  $\text{NO}_x$  is less than 10% in most cases, so the mass balance between the two measurements is closed. Note that the adsorption capacity of the

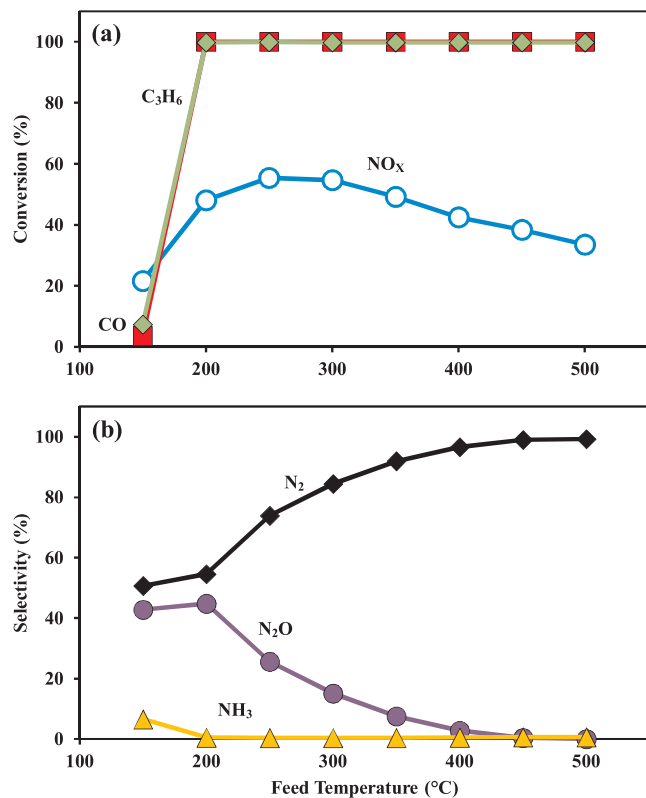


Fig. 3. a,b. (a) Steady state CO,  $\text{NO}_x$ , and  $\text{C}_3\text{H}_6$  conversion vs. feed temperature. (b) Steady state  $\text{N}_2$ ,  $\text{N}_2\text{O}$  and  $\text{NH}_3$  selectivity vs. feed temperature.  $S_N = 1.01$ . Inlet concentrations of  $\text{CO} = 1\%$ ,  $\text{NO} = 500$  ppm,  $\text{C}_3\text{H}_6 = 1000$  ppm,  $\text{H}_2 = 3300$  ppm,  $\text{H}_2\text{O} = 7\%$ ,  $\text{CO}_2 = 10\%$ ,  $\text{O}_2 = 1.08\%$ .

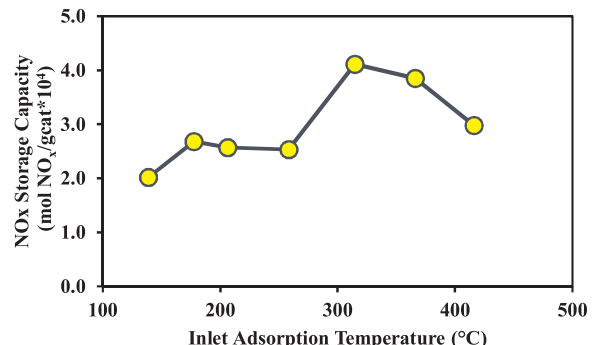


Fig. 4. Lean  $\text{NO}_x$  storage capacity vs. inlet adsorption temperature. Values shown represent the total storage capacity (saturation point) of the TWNSC sample as an average of the adsorption and desorption values calculated for each experiment. Catalyst was pre-reduced at the feed temperature using 2%  $\text{H}_2/\text{Ar}$ . During adsorption, feed consisted of 500 ppm  $\text{NO}$  in 5%  $\text{O}_2$ , and during desorption the feed contained only  $\text{Ar}$ .

TWNSC is bimodal in that there are two local adsorption maxima, consistent with earlier studies of lean NO<sub>x</sub> trap adsorption behavior [33]. This type of behavior suggests storage on two types of sites, namely BaO and either alumina and/or ceria. Note also that H<sub>2</sub>O is not present in these experiments, which leads to a significant increase in NO<sub>x</sub> storage performance when compared to cycling data that contains the full simulated exhaust feed.

### 3.3. Lean-rich cycling experiments

For application in lean combustion exhaust, the transient and cyclic performance of the TWNSC is critical since NO<sub>x</sub> trapping during lean periods and reduction during rich periods must be effective. With cyclic operation, there are several additional operating parameters which present both a challenge and opportunity for optimizing TWNSC performance. In the next several sections the impacts of these parameters on catalyst performance are evaluated. The operating parameters that are varied include the rich time ( $\tau_r$ ), lean time ( $\tau_l$ ), and total cycle time (Eqs. (2a) and 2b). It is convenient to define lean and rich stoichiometric numbers ( $S_{N,l}$ ;  $S_{N,r}$ ), thereby defining a cycle-averaged stoichiometric number ( $S_{N,avg} = (1 - d_r)S_{N,l} + d_rS_{N,r}$ ), which will influence performance. To achieve a prescribed  $S_{N,r}$  the rich phase composition is adjusted through the reductant and O<sub>2</sub> concentrations. Finally, there are additional parameters including the feed temperature ( $T_{feed}$ ) and flowrate.

#### 3.3.1. Baseline cyclic performance

Typical transient cycling data are shown in Fig. 5 for a feed when the temperature ( $T_{feed}$ ) is fixed at 270 °C and lean and rich times are fixed at 25 s [ $\tau_l = 50$  s,  $d_r = \tau_r/\tau_l = 0.5$ ]. The feed gas contains 500 ppm NO, 1% CO, 3300 ppm H<sub>2</sub>, 7% H<sub>2</sub>O, and 10% CO<sub>2</sub> with O<sub>2</sub> switched between 5% during the lean and 0.3% during the rich. These concentrations give  $S_{N,l} = 7.55$  and  $S_{N,r} = 0.45$  and a cycle-averaged value of  $S_{N,avg} = 4.03$ , which is a net-lean feed.

During the lean phase of the cycle, ~80% of the feed NO is trapped on the catalyst based on an analysis of the transient NO<sub>x</sub> data shown in Fig. 5a. There is a short period of duration of ~3 s during which no NO<sub>x</sub> is observed. This is followed by breakthrough and a monotonic increase in NO<sub>x</sub> concentration up to the start of the rich phase, indicating storage of NO<sub>x</sub> throughout the lean cycle. These trends are similar to those reported for the typical storage phase of a lean NO<sub>x</sub> trap [8]. During the lean phase, NH<sub>3</sub> and CO concentrations drop to zero with the NH<sub>3</sub> concentration tail more protracted than CO. The NH<sub>3</sub> tail is due in part to the propensity of NH<sub>3</sub> to adhere to surfaces, delaying its decrease to zero [31]. This effect was proven with a blank tube experiment (data not shown here). It is also noted that with the large excess of O<sub>2</sub> during the lean phase, NO storage generally occurs through its oxidation to NO<sub>2</sub> which stores on trapping sites. The presence of NO<sub>2</sub> and lack of N<sub>2</sub>O during the lean cycle confirms this. Fig. 5b shows the transient profile of the NO<sub>x</sub> components, NO and NO<sub>2</sub>. At the start of the lean phase, there is a slight decrease in NO<sub>2</sub> concentration, due to lean storage of some residual NO<sub>2</sub> present at the end of the rich phase, followed by a minimum before its breakthrough. The NO<sub>2</sub> breakthrough is delayed relative to that of NO. We attribute this to the balance between the rates of NO oxidation to NO<sub>2</sub>, the rate of adsorption, and the sustained feed of NO [31,32].

NO<sub>2</sub> is more readily adsorbed than NO, as has also been shown for lean NO<sub>x</sub> traps [9]. Once NO breakthrough is observed, NO<sub>2</sub>, formed through NO oxidation, continues to adsorb. As the storage sites become saturated, NO oxidation continues and NO<sub>2</sub> breakthrough occurs throughout the remainder of the lean cycle. During this period oxygen is also stored on the catalyst, both on the precious metal crystallites and on/in the ceria phase.

During the rich phase of the cycle the formation of NH<sub>3</sub>, N<sub>2</sub>O, and N<sub>2</sub> involve complex chemistry that depends on many variables including the local catalyst temperature, the relative supply of the various

reacting species, and oxygen coverage on the precious metal crystallites, among other factors [33]. The transient data have three notable features.

First, just after the switch to the rich phase there is a brief increase in the NO<sub>x</sub> concentration, akin to the “NO<sub>x</sub> puff” encountered during regeneration of stored NO<sub>x</sub> on the LNT catalyst [34]. In NSR studies the NO<sub>x</sub> puff is attributed to the difference between the rate of stored nitrite/nitrate decomposition leading to NO<sub>x</sub> release and the rate of NO<sub>x</sub> reduction [10,34]. As regeneration proceeds, less NO<sub>x</sub> is released, allowing the reduction rate to exceed the release rate leading to the eventual decrease in NO<sub>x</sub> concentration. A vanishing NO<sub>x</sub> concentration means that its reduction rate is high relative to the release rate. In some NSR studies the NO<sub>x</sub> concentration during the puff may exceed the feed NO<sub>x</sub> concentration value as the accumulated stored NO<sub>x</sub> desorbs rapidly and with its sustained feed leads to this short-lived additive effect [34].

Second, at about the same time that the NO<sub>x</sub> concentration approaches zero, both NH<sub>3</sub> and CO breakthrough are observed. The NH<sub>3</sub> originates from the reduction of both feed NO and NO<sub>x</sub> stored during the previous lean phase. NH<sub>3</sub> formation behaves as expected during the rich phase, consistent with the steady state and other experiments [35]. The delay in the breakthrough of NH<sub>3</sub> and CO is attributed to their reactions with oxygen and NO<sub>x</sub> stored downstream on ceria and barium components [33]. While there is O<sub>2</sub> in the rich phase inlet gas (0.3%), it is mostly consumed in the net rich environment ( $S_{N,r} = 0.45$ ). Oxygen is stored on the catalyst, most notably on the ceria phase, and is consumed by the feed reductant and the formed NH<sub>3</sub>. Production of NH<sub>3</sub> via H<sub>2</sub> or CO takes place once the Pt surface is fully reduced and less O and NO is available [33,36]. Eventually the surface O is consumed through oxidation of the incoming reductants, and at that point reductant breakthrough is observed. During this period there is a small increase in NO<sub>2</sub>, indicating equilibrium between NO on the surface being reduced or decomposing to form N and O adatoms that could partially form NO<sub>2</sub>. This process evolves spatially; consumption of stored oxygen occurs upstream and moves through the monolith. NH<sub>3</sub> is generated in the oxygen-deficient zone and moves closely behind the CO and H<sub>2</sub> reductant front, and, like H<sub>2</sub>, NH<sub>3</sub> will readily react with stored oxygen (on the ceria phase) and stored NO<sub>x</sub> (on the barium and ceria phases) [33].

The third feature is the small but detectable formation of N<sub>2</sub>O evident early in the rich phase, followed by its decrease to zero. N<sub>2</sub>O is formed due to NO bond scission, generating N adatoms which react with the NO released at the commencement of the regeneration (R14 and R15). Another route is from the reaction between NH<sub>3</sub> formed upstream and NO<sub>x</sub> stored downstream [33]. These data do not show evidence for a second peak which has been reported during NSR studies (e.g., [36]).

The temperature profile for the previously discussed lean and rich cycles is shown in Fig. 5c. As expected, during the lean phase in which combustion of hydrocarbons occurs, there is an increase in the catalyst temperature, peaking at 130 °C relative to the feed temperature. This value corresponds to a peak absolute catalyst temperature of 405 °C. After transitioning to the rich phase, the temperature starts to drop since the large exotherms from combustion are not present. Using this data, a cycle-averaged feed temperature and temperature rise can be calculated, as shown in the figure.

#### 3.3.2. Impact of rich injection intensity

A series of experiments was conducted in which the total amount (volume or moles) of reductant was fixed, while the time over which the reductant was injected was varied. Of interest is whether the reductant injection strategy provides an opportunity to optimize the NO<sub>x</sub> conversion in the case of the standalone TWNSC or the NO<sub>x</sub> conversion and NH<sub>3</sub> selectivity for the TWNSC + SCR system. In a previous LNT study, Kabin et al. [37] varied the rich phase intensity using C<sub>3</sub>H<sub>6</sub> as reductant. More recently Shakya et al. [38] examined the effect of H<sub>2</sub>

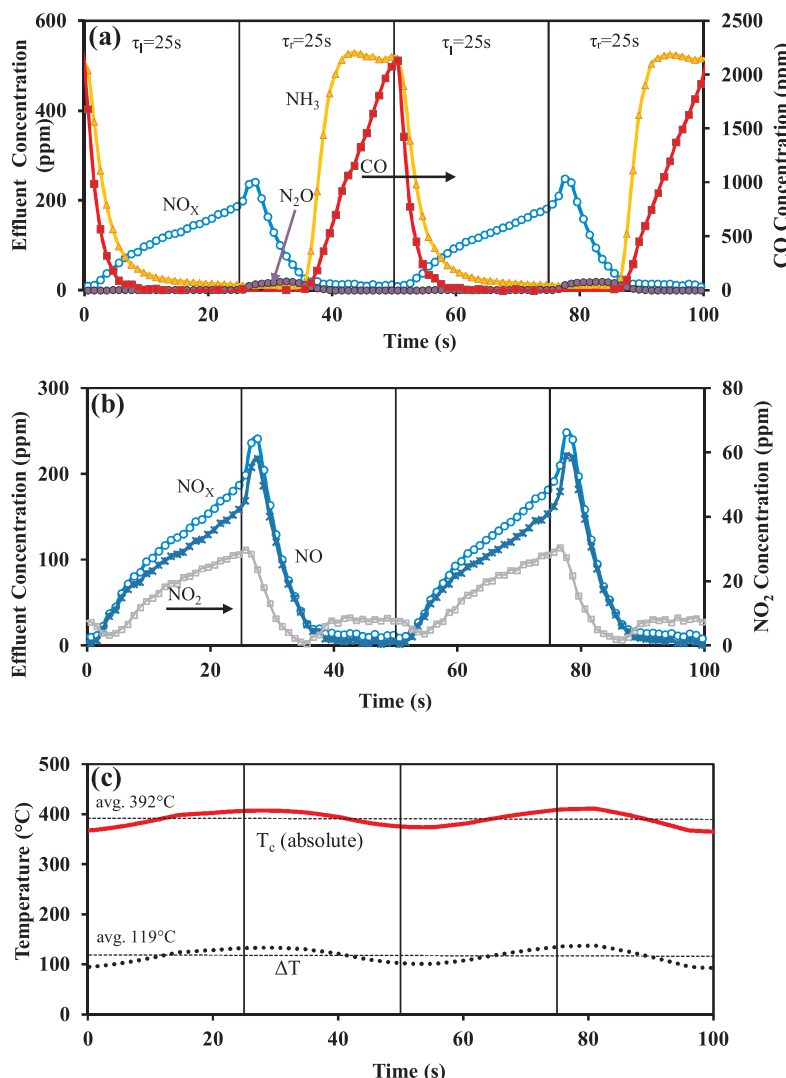


**Fig. 5.** a,b,c. Transient data for lean-rich cycling of TWNSC. (a) Effluent concentration of NO<sub>x</sub>, NH<sub>3</sub>, CO, N<sub>2</sub>O. (b) NO<sub>x</sub> profile as components NO and NO<sub>2</sub>. (c) Catalyst temperature (T<sub>c</sub>, avg = 392 °C) and catalyst temperature rise (ΔT = 119 °C). T<sub>feed</sub> = 270 °C. Lean inlet concentrations (S<sub>N,l</sub> = 7.55): 500 ppm NO, 1% CO, 3300 ppm H<sub>2</sub>, 7% H<sub>2</sub>O, 10% CO<sub>2</sub>, 5% O<sub>2</sub>. Rich inlet concentrations (S<sub>N,r</sub> = 0.45): 500 ppm NO, 1% CO, 3300 ppm H<sub>2</sub>, 7% H<sub>2</sub>O, 10% CO<sub>2</sub>, 0.3% O<sub>2</sub>.

reductant intensity during NO<sub>x</sub> storage and reduction on a Pt/BaO NSR monolith catalyst.

Fig. 6 shows the cycle-averaged results in which the rich duty percentage (100\*d<sub>r</sub>) varies over a 5–70% range for five different feeds during a cycle having a fixed lean duration of τ<sub>l</sub> = 40 s. The rich time (τ<sub>r</sub>) and rich reductant feed volume fraction (C<sub>r</sub>, %v.) was adjusted to maintain a fixed volume of reductant (V<sub>r</sub> = V<sub>CO+H<sub>2</sub></sub> = constant; CO/H<sub>2</sub> = 3) according to

$$C_r = \frac{100 V_r}{d_r \tau_r Q_T} \quad (9)$$

where V<sub>r</sub> is the volume of reductant (CO + H<sub>2</sub>) (in standard cm<sup>3</sup>, or scc), d<sub>r</sub> is the duty fraction of the rich phase, τ<sub>T</sub> is the total cycle time (s), and Q<sub>T</sub> is the standard volumetric flow rate of the feed (scc/s); V<sub>r</sub> and Q<sub>r</sub> are evaluated at standard conditions. Table 2 summarizes the feed parameters for each of the five feeds. For four of the Feeds (I, II, III, IV) the fixed reductant amount is 20 scc while for Feed V the fixed amount is 10 scc. The fixed amount (10 or 20 scc) was varied to access a wider range of rich duty fraction values (for fixed C<sub>r</sub>). The volumetric concentration of O<sub>2</sub> in the rich feed was fixed at three different levels, 0%, 0.27%, and 0.53%. Feeds IV and V represent the case in which the O<sub>2</sub> is varied tightly around the stoichiometric point; i.e. 0.8% O<sub>2</sub> during the lean phase (S<sub>N,l</sub> = 1.24) and 0.53% during the rich phase. The feed

temperature was fixed at 270 °C for four of the five Feeds (I, II, IV, V) and at 470 °C for Feed III.

Fig. 6a and b shows the rich phase stoichiometric number (S<sub>N,r</sub>) and cycle-averaged NO<sub>x</sub> conversion (X<sub>NO<sub>x</sub></sub>) as a function of rich duty percentage, 100d<sub>r</sub> = 100τ<sub>r</sub>/τ<sub>T</sub>. Fig. 6c and d shows the effect of the rich duty percentage on the cycle-averaged CO conversion (X<sub>CO</sub>) and NH<sub>3</sub> selectivity (S<sub>NH<sub>3</sub></sub>), respectively. Fig. 6e similarly shows the NH<sub>3</sub> yield. Each point in the figures represents one cycling experiment.

Examination of Fig. 6 reveals several notable trends. First, the NO<sub>x</sub> conversion (Fig. 6b) for each case generally increases with d<sub>r</sub> up to a value in which a neutral stoichiometric mixture is achieved, i.e. d<sub>r</sub>(S<sub>N,r</sub> = 1). Those values are provided in Table 2 for each feed. For d<sub>r</sub> > d<sub>r</sub>(S<sub>N,r</sub> = 1) the NO<sub>x</sub> conversion decreases as the gas phase becomes net lean. This trend reflects that a rich phase that is both more prolonged and of a lower reductant concentration is more effective than a shorter, more intense pulse, as long as the feed does not become lean (S<sub>N</sub> > 1). For example, for Feed II, X<sub>NO<sub>x</sub></sub> [d<sub>r</sub> = 0.20; τ<sub>T</sub> = 50 s, y<sub>r,CO</sub> + y<sub>r,H<sub>2</sub></sub> = 0.04] = 51%, while X<sub>NO<sub>x</sub></sub> [d<sub>r</sub> = 0.60; τ<sub>T</sub> = 100 s; y<sub>r,CO</sub> + y<sub>r,H<sub>2</sub></sub> = 0.0067] = 67%, with y<sub>r,CO</sub> = 3y<sub>r,H<sub>2</sub></sub>.

Fig. 6b shows that for fixed d<sub>r</sub>, the NO<sub>x</sub> conversion decreases with increasing rich phase O<sub>2</sub> concentration (increasing S<sub>N,r</sub>) and increasing feed temperature (T<sub>f</sub> = 270–470 °C). The former trend underscores that increased reductant enhances NO<sub>x</sub> conversion. The latter trend reflects

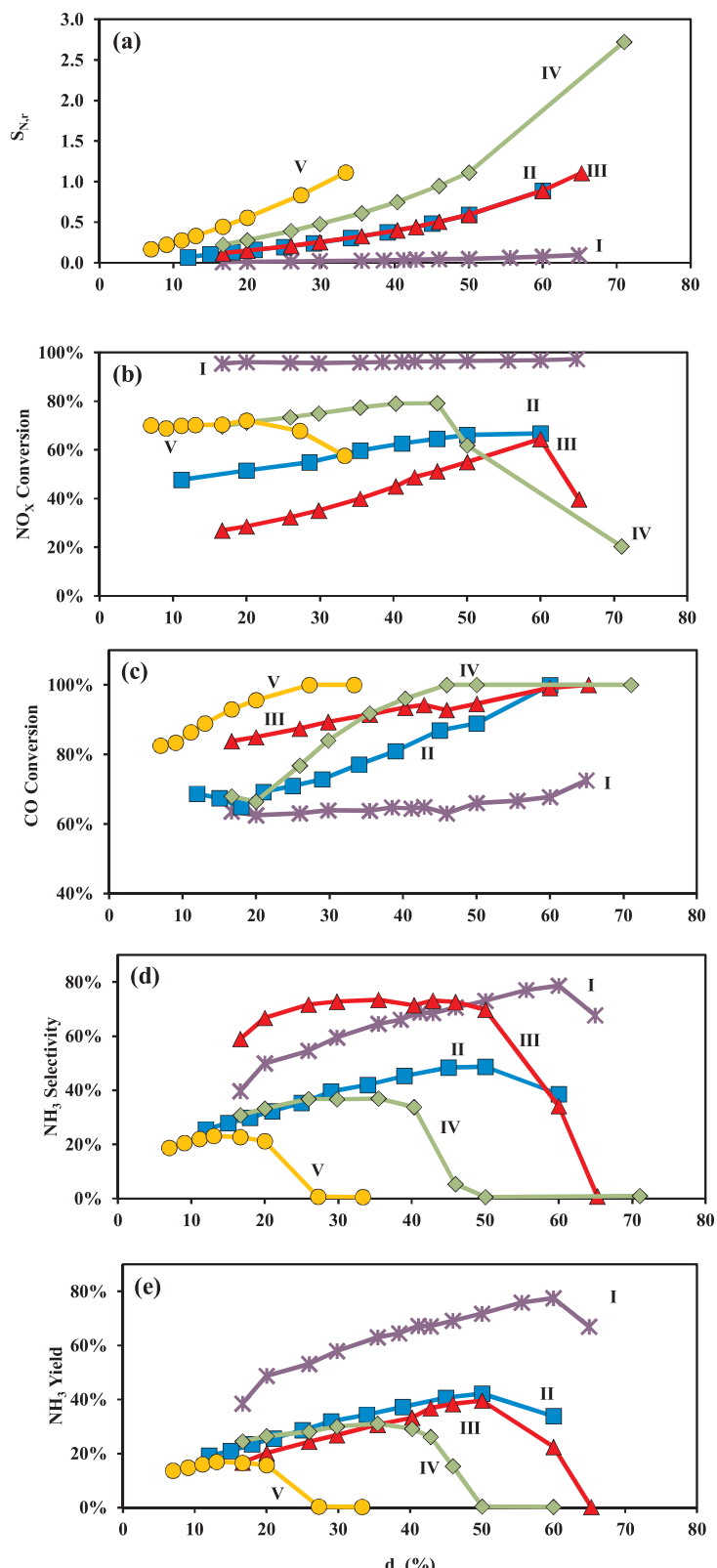


**Fig. 6.** a–e. (a)  $S_{N,r}$  as a function of each duty fraction tested for experiments I–V. (b,c,d,e) Cycle averaged  $NO_x$  and CO conversion,  $NH_3$  yield and selectivity, respectively.  $\tau_l = 40$  s,  $\tau_r$  varied based on  $d_r$  value. Lean inlet concentrations ( $S_N = 1.24$ ): 500 ppm NO, 1% CO, 3300 ppm  $H_2$ , 7%  $H_2O$ , 10%  $CO_2$ , 0.8%  $O_2$ . Rich inlet concentrations: 500 ppm NO, 7%  $H_2O$ , 10%  $CO_2$ , var.  $O_2$ , varied  $CO/H_2$  concentration (total amount of reductant fixed at 10 or 20cc,  $V_{CO}/V_{H_2} = 3$ ).

the detrimental impact on  $NO_x$  storage capacity at high temperature. In contrast to  $NO_x$  conversion, the CO conversion is an increasing function of  $d_r$  and  $T_{feed}$  (Fig. 6c). The  $X_{CO}$  dependence on  $d_r$  reflects that a leaner rich phase benefits the oxidation of CO by gas phase  $O_2$  or stored

oxygen, as expected. The dependence on  $T_{feed}$  simply reflects that an increased temperature increases the rate of oxidation. Fig. 6d shows that  $NH_3$  selectivity is a non-monotonic function of  $d_r$ . This trend reflects the similar trend for  $NO_x$  conversion versus  $d_r$ , although the

**Table 2**

Rich feed description for each of the five duty cycle rich ( $d_r$ ) experiment feeds. For all other parameters:  $\tau_l = 40$  s,  $Q_T = 3000$  sccm; Lean feed constant across all experiments: 500 ppm NO, 1% CO, 3300 ppm H<sub>2</sub>, 7% H<sub>2</sub>O, 10% CO<sub>2</sub>, 0.85% O<sub>2</sub>; Rich feed: 500 ppm NO, 7% H<sub>2</sub>O, 10% CO<sub>2</sub>, Varied O<sub>2</sub>, Varied CO/H<sub>2</sub> in a 3:1 ratio (total volume either 20 or 10 cc).

Feed	% O <sub>2</sub>	T <sub>feed</sub> (°C)	V <sub>CO+H<sub>2</sub></sub> (cc)	d <sub>r</sub> (S <sub>N,r</sub> = 1)
I	0.0	270	20	—
II	0.27	270	20	63%
III	0.27	470	20	63%
IV	0.53	270	20	47%
V	0.53	270	10	30%

maximum S<sub>NH<sub>3</sub></sub> occurs at a lower d<sub>r</sub> value than the d<sub>r</sub> value resulting in a maximum in NO<sub>x</sub> conversion.

The trends in the NH<sub>3</sub> production reflect the balance between NH<sub>3</sub> generation and consumption. A shorter and more intense rich phase is less effective in generating NH<sub>3</sub> as is a rich phase that is not sufficiently rich. At first glance, it may seem counterintuitive that NH<sub>3</sub> selectivity decreases as S<sub>N</sub> decreases, as it was shown for steady state conditions that a rich environment leads to a higher NH<sub>3</sub> production (Fig. 2). However, the pulses for lower d<sub>r</sub> are very short and concentrated which likely leads to a transient poisoning effect of CO on the Pt sites, which inhibits NO reduction to NH<sub>3</sub>. As the rich phase becomes leaner (d<sub>r</sub> and S<sub>N,r</sub> increasing) the selectivity and conversion increase to a maximum value before starting to decrease when the S<sub>N,r</sub> value approaches unity. The prolonged rich phase is insufficiently rich, which decreases the NH<sub>3</sub> generation rate and increases its oxidation rate. It is interesting to note that Feeds II—V follow the same locus of S<sub>NH<sub>3</sub></sub> versus d<sub>r</sub> for decreasing d<sub>r</sub>. This trend suggests a limit on the NH<sub>3</sub> production when the rich phase is sufficiently rich. Indeed, the Feed I results clearly show that a critical variable in these experiments is the O<sub>2</sub> concentration. A rich phase devoid of O<sub>2</sub> gives the highest NH<sub>3</sub> yield over a wide range of rich duty fractions.

### 3.3.3. Impact of feed temperature

The data in Fig. 6 include two sets at identical conditions but two different feed temperatures of 270 and 470 °C, Feeds II and III, respectively. Similar qualitative trends for conversion and selectivity are evident up to a 60% rich duty (S<sub>N,r</sub> < 1), but the magnitudes vary. At 470 °C the NO<sub>x</sub> conversion is lower than it is at 270 °C while the NH<sub>3</sub> selectivity is considerably higher, or equivalently, the N<sub>2</sub> selectivity is much lower (given the relatively negligible N<sub>2</sub>O selectivity). Note however that NH<sub>3</sub> yield (Fig. 6e) is nearly identical regardless of temperature, indicating the amount of NH<sub>3</sub> produced is not affected by temperature under these conditions. By definition, the variation in selectivity is due to the variation in NO<sub>x</sub> conversion. The NO conversion trend is due in part to the decreased NO<sub>x</sub> storage at higher temperatures with a larger fraction coming from direct catalytic conversion during the lean and rich phases. Recall that the steady state data show the NO conversion decreasing over this temperature range for a near-stoichiometric feed (Fig. 3a). On the other hand, the steady-state N<sub>2</sub> selectivity increases with temperature (Fig. 3b). This would appear to contradict the observed opposite trend during cyclic operation (Fig. 6d). Under steady-state conditions the increased N<sub>2</sub> selectivity is a result of the increased rates of NO bond scission and N adatom recombination. The high NH<sub>3</sub> selectivity achieved under cyclic conditions at 470 °C occurs at lower NO<sub>x</sub> conversion and during the rich phase.

In order to better understand the effect of feed temperature on catalyst performance, Fig. 7 shows the NO<sub>x</sub>, N<sub>2</sub>O, NH<sub>3</sub>, and CO effluent concentrations for feed temperatures of 270 °C and 470 °C and a 50% rich duty (lean and rich durations of 40 s). The NO<sub>x</sub> transient data demonstrate that at lower temperatures there is a higher storage of NO<sub>x</sub>, consistent with the NO<sub>x</sub> storage data reported in Fig. 4. This observation explains why there is a higher NO<sub>x</sub> conversion at the lower

temperature. Upon comparing the two profiles, both breakthroughs occur at the same time, although the lower temperature NO<sub>x</sub> profile has a slower approach to saturation than at 470 °C. At higher temperatures the stored NO<sub>x</sub> is not as stable and will undergo desorption and reduction. As shown in Fig. 4, we see that the storage exhibits two maxima, one around 175 °C and one around 300 °C, suggesting that the lean NO<sub>x</sub> storage performance of the catalyst is sensitive the inlet temperature. At 470 °C, the TWNSC is less effective at storing NO<sub>x</sub> under the conditions presented in this paper, but a higher frequency of lean-rich switching (i.e. shorter  $\tau_l$ ) would improve the performance. The individual NO and NO<sub>2</sub> profiles are shown in Fig. 7b. For these conditions, the extent of NO oxidation to NO<sub>2</sub> is dependent on the feed temperature, consistent with the lean NO<sub>x</sub> conversion trends shown in Fig. 3. This behavior suggests that as the operating temperature changes, the cycling protocol can be adjusted to improve both NO<sub>x</sub> conversion and storage efficiency. Additionally, at both feed temperatures the rich phase NO<sub>x</sub> conversion is complete within 20 s of the rich phase feed, suggesting this portion of the cycle is independent of the temperatures used in this study.

The N<sub>2</sub>O transient data show a moderate N<sub>2</sub>O selectivity at 270 °C but a negligible level at 470 °C, consistent with typical N<sub>2</sub>O behavior at low vs. high temperatures for NO<sub>x</sub> storage catalysts. Unlike the results shown earlier for which a wider range of lean/rich switching (7.4 to 0.49) was employed and negligible N<sub>2</sub>O was generated (Fig. 4), at 270 °C the narrow lean/rich switching of 1.24 to 0.60 results in a N<sub>2</sub>O concentration as high as 50 ppm during the rich phase. The formation of N<sub>2</sub>O during the rich phase only occurs during the first 20 s of the cycle, during which time stored O<sub>2</sub> is available. Once the oxygen storage is depleted, NO<sub>x</sub> is fully reduced to N<sub>2</sub>/NH<sub>3</sub>.

The NH<sub>3</sub> transient data are nearly identical at the two feed temperatures. NH<sub>3</sub> breakthrough occurs about 10 s after the start of the rich phase, indicating the consumption of stored oxygen and NO<sub>x</sub> occurring at similar rates in both cases. After breakthrough, the NH<sub>3</sub> concentration approaches 500 ppm, which indicates that NH<sub>3</sub> is the major product in this rich environment, independent of the temperature. NH<sub>3</sub> is not detected during the lean phase. The high selectivity at 270 °C is due to the increased storage of NO<sub>x</sub> in the lean phase, and the yield is the same at both temperatures because the reactor environment is sufficiently rich to fully reduce NO<sub>x</sub> to NH<sub>3</sub> instead of N<sub>2</sub>, likely due to the high concentration of H<sub>2</sub> in the feed. While NH<sub>3</sub> decomposition is expected at higher temperatures, previous studies on similar catalyst compositions have shown that the presence of H<sub>2</sub> during regeneration can inhibit this phenomenon [33]. Additionally, there is a notable difference in the breakthrough profile depending on the temperature. At 270 °C, the NH<sub>3</sub> spikes much faster than at 470 °C, overshooting the feed NO value of 500 ppm, possibly due to the low CO breakthrough during this time as it is still oxidized by stored O<sub>2</sub>. As the CO effluent concentration increases, the NH<sub>3</sub> production rate decreases due to the poisoning effect of CO on the reactive sites. However, at 470 °C, because the CO undergoes water gas shift, there is less poisoning and the NH<sub>3</sub> formation occurs more gradually, approaching 500 ppm as more H<sub>2</sub> is formed.

Finally, the CO transient data also reveal breakthrough at the same point as NH<sub>3</sub> upon oxygen depletion. While the 470 °C profile shows CO leveling off at about 700 ppm, the 270 °C profile shows a progressively increasing concentration during the rich phase. The differences can be attributed to a lower extent of CO conversion by reaction with H<sub>2</sub>O at 270 °C than at 470 °C; i.e. the exothermic water gas shift reaction.

### 3.3.4. Impact of total cycle time

The total cycle time,  $\tau_T$ , is another important operating parameter which must be tuned in conjunction with the rich duty fraction. We report in this section the impact of  $\tau_T$  for several different cases corresponding to feeds of varying stoichiometric numbers, feed temperatures, and reductant types.

Fig. 8 shows the impact of total cycle time on catalyst performance

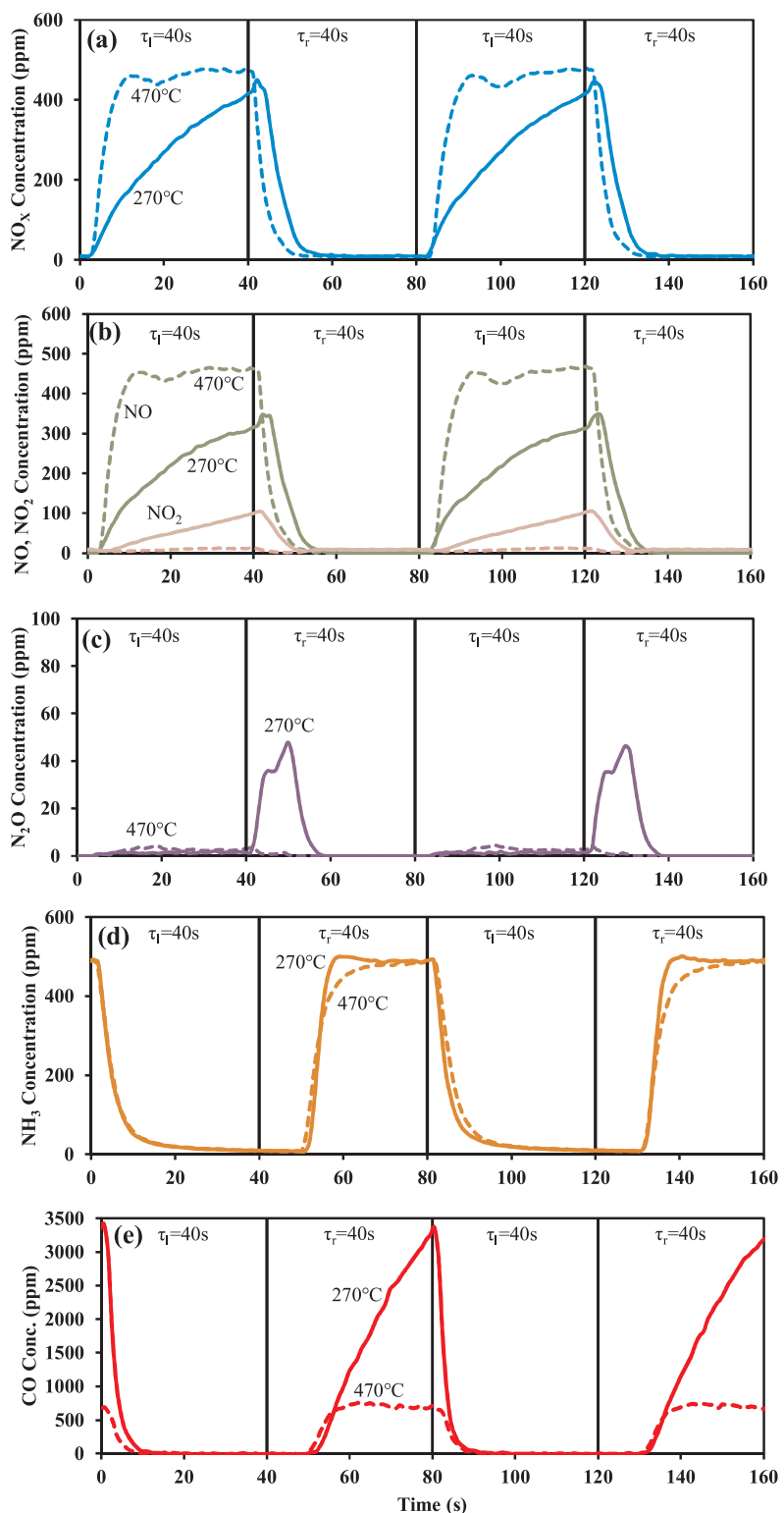


**Fig. 7.** a–e. Transient data for lean-rich cycling selected from  $d_r$  experiments at two feed temperatures and  $d_r = 0.5$ : 270 °C (—), 470 °C (—). (a) NO<sub>x</sub> effluent concentration, (b) NO, NO<sub>2</sub> effluent concentration, (c) N<sub>2</sub>O effluent concentration, (d) NH<sub>3</sub> effluent concentration, (e) CO effluent concentration.  $\tau_l = 40$  s,  $\tau_r = 40$  s. Lean inlet concentrations ( $S_{N,l} = 1.24$ ): 500 ppm NO, 1% CO, 3300 ppm H<sub>2</sub>, 7% H<sub>2</sub>O, 10% CO<sub>2</sub>, 0.8% O<sub>2</sub>. Rich inlet concentrations ( $S_{N,r} = 0.60$ ): 500 ppm NO, 7% H<sub>2</sub>O, 10% CO<sub>2</sub>, 0.27% O<sub>2</sub>, 0.75% CO, 0.25% H<sub>2</sub>.

for two different feed temperatures: 270 °C (Fig. 8a) and 470 °C (Fig. 8b) with a rich duty of 50%. This  $d_r$  value provides a relatively high NO<sub>x</sub> conversion over this temperature range. The lean and rich O<sub>2</sub> concentrations are 5% and 0.37%, respectively, resulting in  $S_{N,l}$  and  $S_{N,r} = 7.4$  and 0.6, respectively. The ANR calculated using Eq. (7) is shown

on the secondary vertical axis.

With the wide disparity in lean and rich compositions a distinct NO<sub>x</sub> conversion maximum is obtained for the 270 °C feed temperature (Fig. 8a). The maximum  $X_{NO_x}$  is 87% for a  $\tau_T = 18$  s. At shorter cycle times the conversion falls off sharply, approaching 47% for  $\tau_T = 4$  s. For

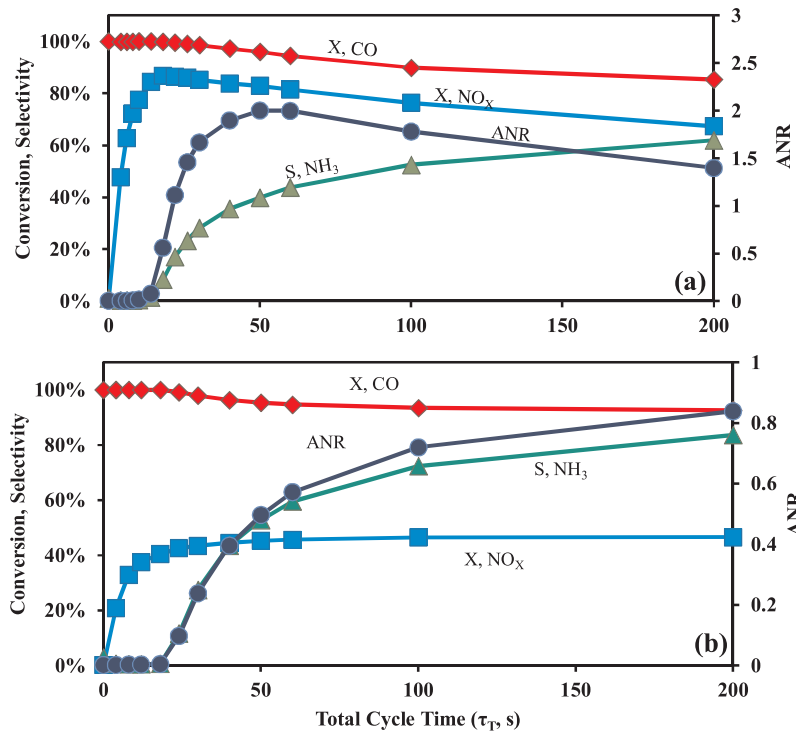


**Fig. 8.** a, b. Cycle-averaged conversion, selectivity and ANR for a Total Cycle Time experiment.  $T_{\text{feed}} =$  (a)  $270^{\circ}\text{C}$ , (b)  $470^{\circ}\text{C}$ . DCR = 50%. Lean inlet concentrations ( $S_{\text{N},\text{l}} = 7.4$ ): 500 ppm NO, 1% CO, 3300 ppm  $\text{H}_2$ , 7%  $\text{H}_2\text{O}$ , 10%  $\text{CO}_2$ , 5%  $\text{O}_2$ . Rich inlet concentrations ( $S_{\text{N},\text{r}} = 0.6$ ): 500 ppm NO, 1% CO, 3300 ppm  $\text{H}_2$ , 7%  $\text{H}_2\text{O}$ , 10%  $\text{CO}_2$ , 0.37%  $\text{O}_2$ . (a) Peak  $\text{NO}_x$  conversion @ 20 s = 87%, ANR at 50 s (2.0). (b) Stable  $\text{NO}_x$  conversion @ 40 s, 44%.

longer cycle times the conversion decreases gradually, approaching 67% at  $\tau_T = 200$  s. A  $\text{NO}_x$  conversion maximum at an intermediate cycle time was first reported by Kabin et al. [37], who examined a lean  $\text{NO}_x$  trap catalyst using propylene as the reductant. They showed that as the cycle time gets shorter, upstream mixing of the lean and rich feeds results in a feed approaching that of a “mixed feed” at steady state. For the current study, with rich and lean duties both 50%, the mixed feed would correspond to a simple arithmetic average of the two; i.e.  $\text{O}_2$  feed concentration =  $(5.0 + 0.37)\% / 2 = 2.69\%$   $\text{O}_2$ . Referring to earlier steady state results in Fig. 2, such a steady lean feed would result in a negligible  $\text{NO}_x$  conversion. Indeed, an extrapolation of  $X_{\text{NO}_x}$  to zero cycle time in Fig. 8a confirms this analysis. In contrast to the  $\text{NO}_x$  conversion, the CO conversion decreases monotonically with cycle time (Fig. 8a) from its maximum value of 100% for  $\tau_T \rightarrow 0$ , while the  $\text{NH}_3$  selectivity monotonically increases from 0 starting at  $\tau_T \sim 14$  s. The CO conversion decline merely reflects that with a more protracted rich phase, more reductant breaks through. In fact, the appearance of  $\text{NH}_3$  at  $\tau_T \sim 14$  s occurs at about the same point as the onset of the decrease in CO conversion, referring back to the transient profiles in Fig. 5a that show the coincident breakthrough of CO and  $\text{NH}_3$ . The declining NO conversion combined with the increase in  $S_{\text{NH}_3}$  result in an ANR having a maximum at an intermediate cycle time; i.e.  $\text{ANR} \sim 2.0$  at  $\tau_T \sim 50$  s. As we expand on later, the existence of the  $\text{NO}_x$  conversion maximum and ANR maximum at two different cycle times poses an interesting operational question.

At  $470^{\circ}\text{C}$  neither the  $\text{NO}_x$  conversion nor the ANR exhibit maxima (Fig. 8b). Under these conditions the  $\text{NO}_x$  storage is much lower. As a result the catalyst performance is effectively a combination of lean and rich operations. The  $\text{NO}_x$  conversion increases sharply from the short cycle mixed-feed limit to  $\sim 47\%$  at long cycle times. This value approaches the weighted average conversion of the lean feed (100%,  $S_{\text{N},\text{r}} = 0.6$ ) and rich feed (0%,  $S_{\text{N},\text{l}} = 7.4$ ) both operated at steady state. The  $\text{NH}_3$  selectivity also increases monotonically from 0 at  $\tau_T = 20$  s to 0.8 at  $\tau_T = 200$  s. The magnitude of ANR is much lower at this rather high feed temperature.

For comparison, another cycle time sweep was carried out with a feed temperature of  $270^{\circ}\text{C}$  but a shorter rich duty of 14%. Fig. 9 shows the same performance metrics when the lean-rich switching is confined

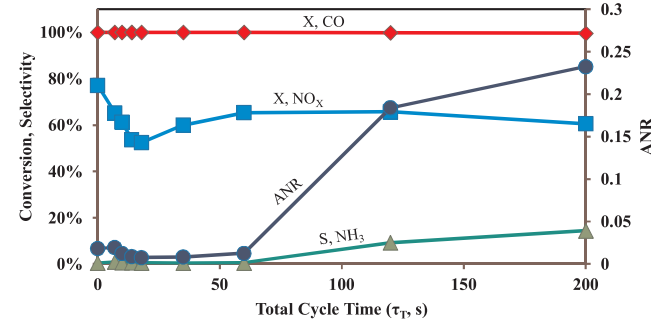


**Fig. 9.** Cycle-averaged conversion, selectivity and ANR for a Total Cycle Time experiment.  $T_{\text{feed}} = 270^{\circ}\text{C}$ . DCR = 14%. Lean inlet concentrations ( $S_{\text{N},\text{l}} = 1.18$ ): 500 ppm NO, 1% CO, 3300 ppm  $\text{H}_2$ , 7%  $\text{H}_2\text{O}$ , 10%  $\text{CO}_2$ , 0.8%  $\text{O}_2$ . Rich inlet concentrations ( $S_{\text{N},\text{r}} = 0.83$ ): 500 ppm NO, 1% CO, 3300 ppm  $\text{H}_2$ , 7%  $\text{H}_2\text{O}$ , 10%  $\text{CO}_2$ , 0.53%  $\text{O}_2$ .

to a  $S_{\text{N}}$  range between 1.18 (lean) and 0.83 (rich) and a feed temperature of  $270^{\circ}\text{C}$ . The  $\text{NO}_x$  conversion has two extrema over the  $\tau_T$  range of 0–200 s total cycle time; a maximum of 77% for  $\tau_T = 0$  s (obtained with a mixed feed and  $S_{\text{N}} \sim 1.005$ ), and a minimum of 52% at  $\tau_T = 18$  s. For the longest cycle time of  $\tau_T = 200$  s,  $X_{\text{NO}_x}$  is  $\sim 61\%$ . That the highest conversion is encountered with the continuously-fed mixed feed indicates that cycling is actually detrimental for this near-stoichiometric feed. The CO conversion exceeds 99% over the entire range of cycle times.  $\text{NH}_3$  generation under these conditions is quite low with a maximum of only 14% selectivity achieved at a cycle time of 200 s while the net  $\text{NH}_3$  generation is negligible for cycle times less than 60 s.

### 3.3.5. Impact of reductant type

Most of the experiments presented up to this point have involved a reductant feed containing CO and  $\text{H}_2$ . In practice, the feed also contains hydrocarbons, so it is useful to assess the TWNSC performance when each of the three reductant types is present. Fig. 10 shows the results for a three-reductant feed (Fig. 10a) and a feed containing  $\text{C}_3\text{H}_6$  as the sole reductant (Fig. 10b). Both experiments were conducted at the same feed temperature of  $270^{\circ}\text{C}$  while the rich duty was fixed at 50%. The  $\text{C}_3\text{H}_6$

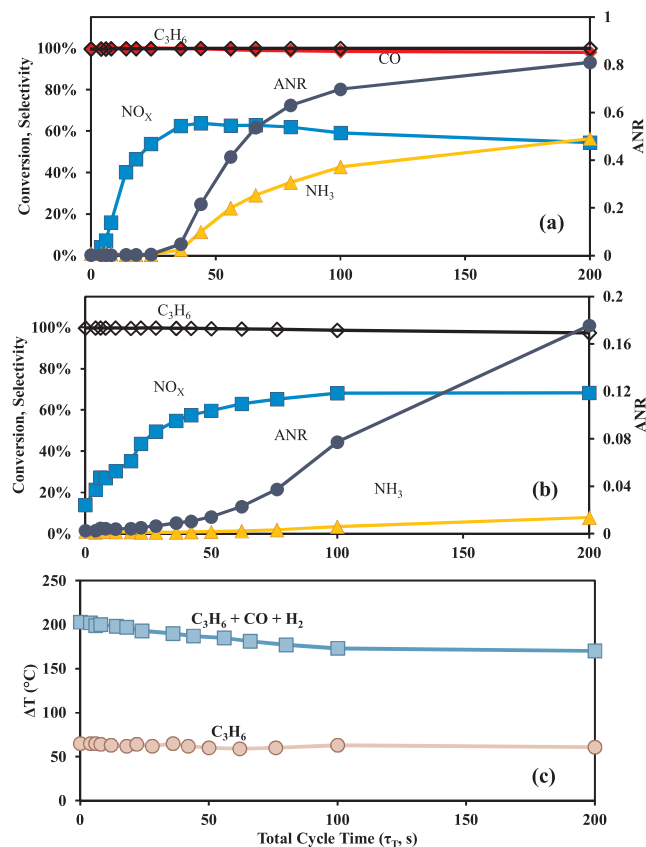


**Fig. 10.** a,b,c. (a,b) Cycle-averaged conversion, selectivity and ANR for a set of Total Cycle Time experiments.  $T_{\text{feed}} = 270^{\circ}\text{C}$ . DCR = 50%. Lean inlet concentrations ( $S_{N,\text{l}} \sim 7.4$ ): a: 500 ppm NO, 1% CO, 3300 ppm H<sub>2</sub>, 1000 C<sub>3</sub>H<sub>6</sub>, 7% H<sub>2</sub>O, 10% CO<sub>2</sub>, 8.4% O<sub>2</sub>; b: 500 ppm NO, 1000 ppm C<sub>3</sub>H<sub>6</sub>, 7% H<sub>2</sub>O, 10% CO<sub>2</sub>, 3.4% O<sub>2</sub>. Rich inlet concentrations ( $S_{N,\text{r}} \sim 0.8$ ): a: 500 ppm NO, 1% CO, 3300 ppm H<sub>2</sub>, 1000 ppm C<sub>3</sub>H<sub>6</sub>, 7% H<sub>2</sub>O, 10% CO<sub>2</sub>, 0.9% O<sub>2</sub>; b: 500 ppm NO, 1000 ppm C<sub>3</sub>H<sub>6</sub>, 7% H<sub>2</sub>O, 10% CO<sub>2</sub>, 0.35% O<sub>2</sub>. (a) Peak NO<sub>x</sub> conversion @ 44 s = 64%. (c) Cycle averaged catalyst temperature rise ( $\Delta T$ ) for case a (C<sub>3</sub>H<sub>6</sub> + CO + H<sub>2</sub>) and b (C<sub>3</sub>H<sub>6</sub>).

**Table 3**

Concentration of reductants and O<sub>2</sub> during the lean and rich phase used in the reductant analysis cycling experiments explained in Fig. 11. In the cells labeled “Lean/Rich,” the corresponding concentration was used in both lean and rich phases.

Set:	CO	H <sub>2</sub>	C <sub>3</sub> H <sub>6</sub>	CO + H <sub>2</sub>	CO + H <sub>2</sub> + C <sub>3</sub> H <sub>6</sub>
O <sub>2</sub>	Lean	5%	5%	5%	5%
	Rich	0.53%	0.53%	0.53%	0.9%
CO	Lean/Rich	1.33%	–	–	1%
H <sub>2</sub>	Lean/Rich	–	1.33%	–	0.33%
C <sub>3</sub> H <sub>6</sub>	Lean/Rich	–	–	0.147%	–

concentration in the lean and rich phases for each experiment was fixed at 1000 ppm while the CO and H<sub>2</sub> concentrations were 1% and 3300 ppm, respectively, for the three-reductant feed. The O<sub>2</sub> concentrations in the rich and lean phases were adjusted to ensure that the  $S_{N,\text{r}}$  and  $S_{N,\text{l}}$  were fixed at 7.4 and 0.8, respectively. Table 3 reports the feed concentrations. Note that the exothermic heat effects (Fig. 10c) are larger for the three-reductant feed.

For the three-reductant feed results (Fig. 10a) there is a distinct maximum in the NO<sub>x</sub> conversion (~64%) at  $\tau_{\text{T}} \sim 44$  s. At the cycle time limits of 4 s (mixed feed) and 200 s, NO<sub>x</sub> conversion is ~0.2 and ~56%, respectively. In contrast, for the C<sub>3</sub>H<sub>6</sub> only feed (Fig. 10b) the NO<sub>x</sub> conversion increases monotonically from ~12% at  $\tau_{\text{T}} = 4$  s to ~68% at  $\tau_{\text{T}} = 200$  s. The comparison shows that C<sub>3</sub>H<sub>6</sub> is more effective

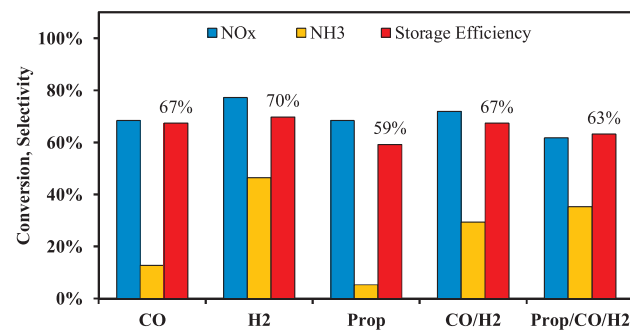


**Fig. 11.** NO<sub>x</sub> conversion and NH<sub>3</sub> selectivity for various combinations of reductant in the feed.  $T_{\text{feed}} = 270^{\circ}\text{C}$ . Total cycle time, 80 s,  $\tau_{\text{l}} = 40$  s,  $\tau_{\text{r}} = 40$  s. All feeds contained 10% CO<sub>2</sub>, 7% H<sub>2</sub>O, 500 ppm NO, and varying concentrations of CO, H<sub>2</sub>, C<sub>3</sub>H<sub>6</sub>, and O<sub>2</sub> to achieve  $S_{N,\text{l}} = 7.6$  and  $S_{N,\text{r}} = 0.83$  (see Table 3).

in reducing NO<sub>x</sub> than the three-component mixture for shorter cycle times ( $\tau_{\text{T}} < \sim 10$  s) and nearly as effective for longer cycle times. The short cycle time difference may be due to CO inhibition as was discussed earlier (Figs. 2 and 3). Each case shows nearly complete conversion of the reductant over the entire range of cycle times. This is the result of the overall lean conditions ( $S_{\text{N}} \sim (7.4 + 0.8)/2 = 4.1$ ). On the other hand, a large difference is evident in NH<sub>3</sub> generation under these conditions. Clearly CO and H<sub>2</sub> are much more effective in generating NH<sub>3</sub>. Corresponding to these trends is a much higher ANR for the three-reductant feed than the propylene-only feed. This is not surprising given that NO conversion by H<sub>2</sub> to NH<sub>3</sub> is very effective under these conditions.

Fig. 11 shows the effect of using various combinations of reductants on the cycle-averaged NO<sub>x</sub> conversion and NH<sub>3</sub> selectivity. To enable a meaningful comparison, the cycle time and rich duty ( $\tau_{\text{T}} = 80$  s;  $d_{\text{r}} = 0.5$ ), feed temperature (270 °C) and stoichiometric numbers for both the lean ( $S_{N,\text{l}} = 7.6$ ) and rich phases ( $S_{N,\text{r}} = 0.83$ ) were fixed. Species concentrations were adjusted to maintain the fixed  $S_{N,\text{l}}$  and  $S_{N,\text{r}}$  values. Overall, the conversion of NO<sub>x</sub> varies less with the type of reductant in the feed than does the NH<sub>3</sub> selectivity.  $X_{\text{NO}_x}$  varies between 62% (mixture of three reductants) and 77% (H<sub>2</sub> only) while  $S_{\text{NH}_3}$  varies between 45% (H<sub>2</sub> only) and 5% (C<sub>3</sub>H<sub>6</sub>). In maximizing both NO<sub>x</sub> conversion and NH<sub>3</sub> selectivity, H<sub>2</sub> is the most effective reductant [26,30]. Any feed that contains H<sub>2</sub> increased the NH<sub>3</sub> selectivity, consistent with the discussion in previous sections regarding the enhancement of H<sub>2</sub> on NH<sub>3</sub> selectivity.

To better understand these trends, Fig. 12a shows the transient effluent NO<sub>x</sub> concentration for one lean-rich cycle using each of the reductant feeds. Each of the NO<sub>x</sub> profiles are qualitatively similar, i.e., during the lean phase there is a brief period of complete NO<sub>x</sub> trapping followed by NO<sub>x</sub> breakthrough with a gradual increase; during the rich phase there is a NO<sub>x</sub> spike followed by a sharp decrease. Overall the data show that H<sub>2</sub> is the most effective reductant, followed by CO/H<sub>2</sub>. The NO<sub>x</sub> conversion is primarily affected by two factors, the lean storage and the intensity of the NO<sub>x</sub> spike that occurs during the lean-rich transition. An estimate of the lean NO<sub>x</sub> storage efficiency ( $\eta_{\text{L}}$ ), determined using Eq. (8), is highest for H<sub>2</sub> (70%) and lowest for propylene (59%). The C<sub>3</sub>H<sub>6</sub> data shows the steepest NO<sub>x</sub> breakthrough during the first half of the lean phase while all of the other feeds have nearly identical NO<sub>x</sub> breakthroughs during this period. Interestingly, the C<sub>3</sub>H<sub>6</sub>-only NO<sub>x</sub> breakthrough intersects the three-component feed near the end of the lean period. The NO<sub>x</sub> concentration during the rich phase shows greater disparity in the several cases. For feeds containing CO, the NO<sub>x</sub> spike is most pronounced. This would appear to indicate that CO inhibits the regeneration. The comparison of the CO-only and H<sub>2</sub>-only or the propylene-only and the three component feeds underscore this point.

Fig. 12b shows the corresponding transient mid-point catalyst

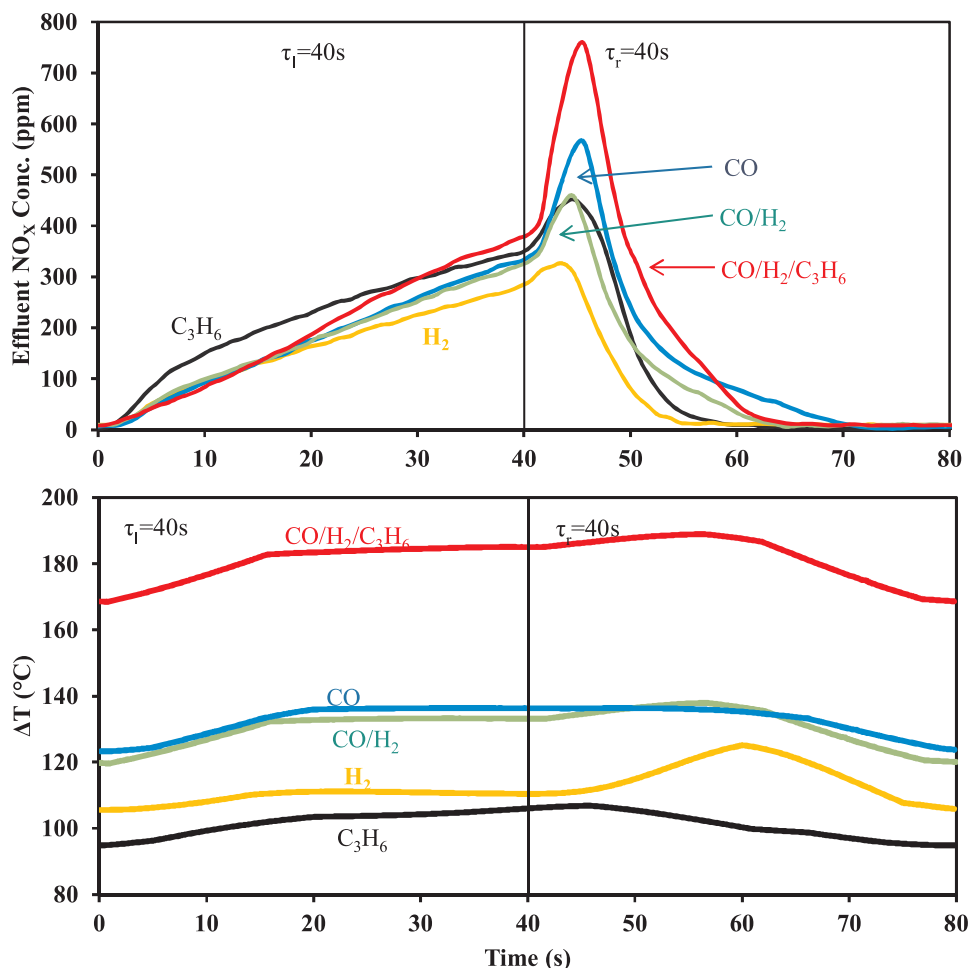


**Fig. 12.** a,b. (a) Transient NO<sub>x</sub> concentration profile for one lean/rich cycle for various combinations of reductants, taken from raw data of experiments described in Fig. 10. (b) Temperature rise of one cycle for each of the five feeds described in Fig. 10.  $\tau_l = 40$  s,  $\tau_r = 40$  s,  $T_{feed} = 270$  °C,  $S_{N,l} = 7.6$ ,  $S_{N,r} = 0.83$  (see Table 3).

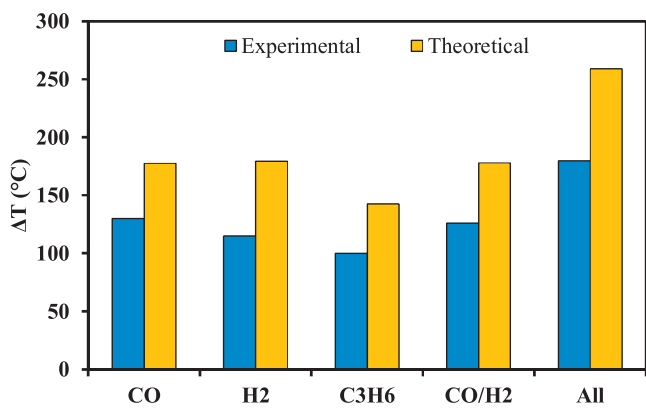


**Fig. 13.** Comparison of cycle-averaged catalyst temperature rise to theoretical values calculated according to Eq. (10).

temperature. For all feeds, there is a gradual increase during the lean phase (oxidation), followed by a decrease during the rich phase (reduction). The lowest temperature rise is encountered with the propylene-only case, followed by the H<sub>2</sub> case, and then the CO containing cases. The highest temperature rise is seen with the three-reductant feed. Fig. 13 shows the measured, cycle-averaged temperature rise for each case compared to an estimate for the theoretical steady-state value using the following expression for the adiabatic temperature rise:

$$\Delta T = \frac{-\Delta H_{rxn} X C_r}{C_p} \quad (10)$$

where  $\Delta H_{rxn}$  is the heat of combustion of the reductant, X is the conversion,  $C_r$  is the concentration (volume percentage), and  $C_p$  is the heat capacity of the feed gas. As shown in the figure, there is agreement in the trend between the temperature rise of individual species and the reductant mixtures. However, there is an overall difference in magnitude between the measured and theoretical values, most attributed to reactor heat losses. The observed conversion of each reductant mixture in this set of experiments is more than 98%. As such, the temperature rise values are attributed to variations in reductant concentration and the heat of combustion of each species.

### 3.4. Optimal operation

The TWNSC performance results suggest that system optimization is nontrivial. The manipulated operating parameters include the cycle time, rich duty fraction, rich phase O<sub>2</sub> concentration, and feed temperature. The choice of which performance metric is the most critical depends on intended application of the TWNSC. For the standalone TWNSC, operating conditions should be selected that maximize the NO<sub>x</sub> conversion, reductant conversion, and N<sub>2</sub> selectivity while minimizing the reductant usage. In contrast, for the TWNSC followed by a SCR, the NO<sub>x</sub> conversion should be balanced across both reactors to take advantage of the lower cost SCR. In that case the rich phase operating conditions should be selected that give a NO<sub>x</sub> conversion approaching 50% and a NH<sub>3</sub> selectivity as high as possible to impact

downstream SCR, i.e. ANR  $\sim 1$  [20,21]. Identifying the precise operating conditions would require a detailed multi-variable optimization.

To illustrate the optimization strategy, it is instructive to evaluate the case when cycling is done with widely different feed compositions. Fig. 8a shows such a case using CO + H<sub>2</sub> as the reductant mixture that might represent a lean gasoline application. In those experiments the data reveal the existence of two maxima obtained at different cycle time values. The first maximum is of the NO<sub>x</sub> conversion while the second is of the ANR. Selecting the NO<sub>x</sub> conversion maximum (87%) as the operating point for the standalone TWNSC would require a total cycle time of  $\sim 18$  s at the duty rich fraction of 50%. Under these conditions the NH<sub>3</sub> selectivity is rather low ( $\sim 20\%$ ) and the CO conversion is very high ( $\sim 99.9\%$ ). On the other hand, for the TWNSC + SCR configuration, there are two potential operating points at which ANR  $\sim 1$ . If a downstream SCR catalyst is available, as mentioned earlier the optimal ANR value is unity. The first is to the left of the ANR maximum, while the second is well to the right of the ANR maximum (e.g., at  $\tau_T \sim 20$  s and at  $\tau_T \sim 200$  s, respectively). The latter would appear to be the better choice as X<sub>NO<sub>x</sub></sub>  $\sim 67\%$  and S<sub>NH<sub>3</sub></sub>  $\sim 62\%$  which are closer to the desired optimal values of 50% and 100%, respectively. However, the CO conversion at this cycle time is 85%, an issue that still needs to be addressed for a TWNSC system. Another potential operating point might be at the ANR maximum which occurs for  $\tau_T \sim 50$  s. In this case the NO<sub>x</sub> conversion is  $\sim 83\%$  and the NH<sub>3</sub> selectivity is  $\sim 44\%$ . Moreover, the CO conversion is 96%. Obviously, this illustration over-simplifies the optimization but it does provide insight into the main issues.

The catalyst performance is qualitatively different at a higher feed temperature (Fig. 8b). Because the lean NO<sub>x</sub> storage is poor at 470 °C, the cycle-averaged conversion stabilizes after only 40 s instead of exhibiting a maximum, indicating that even with longer lean periods, the NO<sub>x</sub> breaks through and increases to its feed concentration within 40 s. Another key difference at the higher feed temperature is that the NH<sub>3</sub> selectivity and ANR steadily increase. The ANR value does not approach 1.0 in these conditions, mostly due to the decrease in NO<sub>x</sub> conversion at higher feed temperature. Since the NO<sub>x</sub> conversion stabilizes, we would expect NH<sub>3</sub> selectivity to increase because a longer rich period generates more NH<sub>3</sub>. To optimize this system, a total cycle time of 40 s would be a good choice leading to 45% NO<sub>x</sub> conversion and a reasonable NH<sub>3</sub> selectivity (ANR of 0.4, and a CO conversion of 96%). A higher cycle time would lead to better NH<sub>3</sub> yield, but long cycle times are much less practical for engine operation, and the additional loss of CO conversion is problematic.

#### 4. Conclusions

A systematic study of the performance of a commercial three-way NO<sub>x</sub> storage catalyst (TWNSC) was conducted. The study provides insight about the potential for its use in lean-burn gasoline vehicle exhaust as a standalone unit or the first of two units in tandem with a downstream SCR. The steady-state performance expectedly shows the demarcation between rich and lean such that within a narrow window around the stoichiometric neutral point high conversion of CO, hydrocarbon (C<sub>3</sub>H<sub>6</sub>), and NO can be achieved. In general, CO and C<sub>3</sub>H<sub>6</sub> conversions increase with temperature and stoichiometric number S<sub>N</sub>, while NO<sub>x</sub> conversion and NH<sub>3</sub> production decrease with increasing temperature and S<sub>N</sub>.

The performance features under lean/rich cycling are amenable for either standalone TWNSC or the tandem TWNSC + SCR configuration. The cycling protocol may be designed to achieve a high NO<sub>x</sub> conversion and N<sub>2</sub> selectivity, but this will generally require reductant exceeding a threshold value that leads to difficulty in avoiding NH<sub>3</sub> and CO slip whereas insufficient reductant will lead to an inadequate NO<sub>x</sub> conversion. The concentrations of reductant and O<sub>2</sub>, duration of the rich pulse (duty fraction), and cycle time may be tuned to achieve a desired NO<sub>x</sub> conversion and/or NH<sub>3</sub> selectivity. If there is a large disparity in the lean/rich ratio over the cycle, the NO<sub>x</sub> conversion exhibits a maximum

value at an intermediate cycle time, as does the ammonia to NO<sub>x</sub> ratio. Optimization should be possible for a particular application that maximizes the NO<sub>x</sub> conversion and reductant utilization. Clearly, the optimization would benefit from modeling, which will be discussed in a forthcoming companion publication.

#### Acknowledgements

We acknowledge the financial support of this research by FCA US LLC (Auburn Hills, Michigan) along with helpful discussions with FCA US LLC researchers Drs. Kiran Premchand, Vence Easterling, Yang Zheng, and Mr. Craig Dimaggio.

#### References

- U.S. Energy Information Administration: U.S. Job Market and Automotive Sales Trends Support Growth in Gasoline Use, (2015) . September <http://www.eia.gov/todayinenergy/detail.cfm?id=22932>.
- EPA: Light-Duty Vehicles and Trucks Emission Standards, (2016) . March <https://www.epa.gov/emission-standards-reference-guide/light-duty-vehicles-and-trucks-emission-standards>.
- K. Packham, Lean-Burn Engine Technology Increases Efficiency, Reduces NOX Emissions, Cummins internal publication, 2007, <http://power.cummins.com/sites/default/files/literature/technicalpapers/PT-7009-LeanBurn-en.pdf>.
- J. Wang, H. Chen, Z. Hu, M. Yao, Y. Li, A review on the Pd-based three-way catalyst, *Catal. Rev.: Sci. Eng.* 57 (2015) 79–144.
- M. Shelef, K. Otto, J. Gandhi, The oxidation of CO and O<sub>2</sub> and by NO on supported chromium oxide and other metal oxide catalysts, *J. Catal.* 12 (1968) 361–365.
- R. Burch, P.J. Millington, Selective reduction of nitrogen oxides by hydrocarbons under lean-burn conditions using supported platinum group metal catalysts, *Catal. Today* 26 (1995) 185–206.
- M. Twigg, Progress and future challenges in controlling automotive exhaust gas emissions, *Appl. Catal. B* 70 (2007) 2–15.
- N. Takahashi, H. Shinjoh, T. Suzuki, The new concept 3-way catalyst for automotive lean-burn engines: NO<sub>x</sub> storage and reduction catalyst, *Catal. Today* 27 (1996) 63–69.
- M. Harold, NO<sub>x</sub> storage and reduction in lean burn vehicle emission control: a catalytic engineer's playground, *Curr. Opin. Chem. Eng.* 1 (2012) 1–9.
- K. Kabin, P. Khanna, R. Muncrief, V. Medhekar, M.P. Harold, Monolith and TAP reactor studies of NO<sub>x</sub> storage on Pt/BaO/Al<sub>2</sub>O<sub>3</sub>: elucidating the mechanistic pathways and roles of Pt, *Catal. Today* 114 (2006) 72–85.
- W.S. Epling, J. Parks, G. Campbell, A. Yezerski, N.W. Currier, Further evidence of multiple NO<sub>x</sub> sorption sites on NO<sub>x</sub> storage/reduction catalysts, *Catal. Today* 96 (2004) 21–30.
- A. Kumar, M.P. Harold, V. Balakotaiah, Isotopic studies of NO<sub>x</sub> storage and reduction on Pt/BaO/Al<sub>2</sub>O<sub>3</sub> catalyst using temporal analysis of products, *J. Catal.* 270 (2010) 214–223.
- J. Anderson, B. Bachiller-Baeza, M. Fernandez-Garcia, Role of Pt in Pt/Ba/Al<sub>2</sub>O<sub>3</sub> NO<sub>x</sub> storage and reduction traps, *Phys. Chem. Chem. Phys.* 5 (2003) 4418.
- J. Barbier, D. Duprez, Steam effects in three-way catalysis, *Appl. Catal. B* 4 (1994) 105–140.
- G. Liu, G. Pu-Xian, A review of NO<sub>x</sub> storage/reduction catalysts: mechanism, materials and degradation studies, *Catal. Sci. Technol.* 1 (2011) 552–568.
- J.Y. Luo, W.S. Epling, New insights into the promoting effect of H<sub>2</sub>O on a model Pt/Ba/Al<sub>2</sub>O<sub>3</sub> NSR catalyst, *Appl. Catal. B* 97 (2010) 236–247.
- M. Colombo, I. Nova, E. Tronconi, A comparative study of the NH<sub>3</sub>-SCR reactions over a Cu-zeolite and a Fe-zeolite, *Catal. Today* 151 (2010) 223–230.
- Y. Zheng, Y. Liu, M.P. Harold, D. Luss, LNT-SCR dual-layer catalysts optimized for lean NO<sub>x</sub> reduction by H<sub>2</sub> and CO, *Appl. Catal. B* 148–149 (2014) 311–321.
- J. Theis, M. Dearth, R.W. McCabe, LNT + SCR Systems Optimized for NO<sub>x</sub> Conversion on Diesel Applications, SAE International, 2011.
- M. Li, V. Easterling, M.P. Harold, Towards optimal operation of sequential NO<sub>x</sub> storage and reduction and selective catalytic reduction, *Appl. Catal. B. Environ.* 184 (2016) 364–380.
- M. Li, V. Easterling, M.P. Harold, Spatio-temporal features of lean NO<sub>x</sub> reduction the sequential NO<sub>x</sub> storage and reduction and selective catalytic reduction reactor system, *Catal. Today* 267 (2016) 177–191.
- Y. Ikeda, K. Sobue, S. Tsuji, S. Matsumoto, Development of NO<sub>x</sub> Storage-Reduction Three-Way Catalyst for D-4 Engines, SAE International, 1999.
- J. Theis, J. Kim, G. Cavataio, Passive TWC+SCR Systems for Satisfying Tier 2, Bin 2 Emission Standards on Lean-Burn Gasoline Engines, SAE International, 2015, p. 8.
- C.D. DiGiulio, J.A. Pihl, J.E. Parks II, M.D. Amirdis, T.J. Toops, Passive-ammonia selective catalytic reduction (SCR): understanding NH<sub>3</sub> formation over close-coupled three-way catalysts (TWC), *Catal. Today* 231 (2014) 33–45.
- L. Lietti, N. Artioli, L. Righini, L. Castoldi, P. Forzatti, Pathways for N<sub>2</sub> and N<sub>2</sub>O formation during the reduction of NO<sub>x</sub> over Pt-Ba/Al<sub>2</sub>O<sub>3</sub> LNT catalysts investigated by labeling isotopic experiments, *Ind. Eng. Chem. Res.* 51 (2012) 7597–7605.
- J. Xu, R. Clayton, V. Balakotaiah, M.P. Harold, Experimental and microkinetic modeling of steady-state NO reduction by H<sub>2</sub> on Pt/BaO/Al<sub>2</sub>O<sub>3</sub> monolith catalysts, *Appl. Catal. B* 77 (2007) 395–408.

[27] S. Voltz, C. Morgan, D. Liederman, S. Jacob, Kinetic study of carbon monoxide and propylene oxidation on platinum catalysts, *Ind. Eng. Chem. Prod. Res. Dev.* 12 (1973) 294–301.

[28] R. Burch, A.A. Shestov, J.A. Sullivan, A steady-state isotopic transient kinetic analysis of the NO/O<sub>2</sub>/H<sub>2</sub> reaction over Pt/SiO<sub>2</sub> catalysts, *J. Catal.* 188 (1999) 69–82.

[29] J.M. Dasch, Nitrous oxide emissions from vehicles, *J. Air Waste Manage.* 42 (2012) 63–67.

[30] I. Nova, L. Lietti, L. Castoldi, E. Tronconi, P. Forzatti, New insights in the NO<sub>x</sub> reduction mechanism with H<sub>2</sub> over Pt-Ba/y-Al<sub>2</sub>O<sub>3</sub> lean NO<sub>x</sub> trap catalysts under near-isothermal conditions, *J. Catal.* 239 (2006) 244–254.

[31] D. Bhatia, R. Clayton, M.P. Harold, V. Balakotaiah, A global kinetic model for NO<sub>x</sub> storage and reduction on Pt/BaO/Al<sub>2</sub>O<sub>3</sub> monolithic catalysts, *Catal. Today* 147 (2009) 250–256.

[32] D. Bhatia, R.W. McCabe, M.P. Harold, V. Balakotaiah, Experimental and kinetic study of NO oxidation on model Pt catalysts, *J. Catal.* 266 (2009) 106–119.

[33] R.D. Clayton, M.P. Harold, V. Balakotaiah, Performance features of Pt/BaO lean NO<sub>x</sub> trap with hydrogen as reductant, *AIChE J.* 55 (2009) 687–700.

[34] R. Muncrief, K. Kabin, M.P. Harold, NO<sub>x</sub> storage and reduction with propylene on Pt/BaO/Alumina, *AIChE J.* 50 (2004) 2526–2540.

[35] R. Clayton, M.P. Harold, V. Balakotaiah, NO<sub>x</sub> storage and reduction with H<sub>2</sub> on Pt/BaO/Al<sub>2</sub>O<sub>3</sub> monolith: spatio-temporal resolution of product distribution, *Appl. Catal. B* 84 (2008) 616–630.

[36] D. Mracek, P. Koci, J.S. Choi, W.P. Partridge, New operation strategy for driving the selectivity of NO<sub>x</sub> reduction to N<sub>2</sub>, NH<sub>3</sub> or N<sub>2</sub>O during lean/rich cycling of a lean NO<sub>x</sub> trap catalyst, *Appl. Catal. B* 182 (2015) 109–114.

[37] K. Kabin, R. Muncrief, M.P. Harold, NO<sub>x</sub> storage and reduction on a Pt/BaO/alu-mina monolithic storage catalyst, *Catal. Today* 96 (2004) 79–89.

[38] B. Shakya, M.P. Harold, V. Balakotaiah, Effect of cycle time on NH<sub>3</sub> generation on Low Pt dispersion Pt/BaO/Al<sub>2</sub>O<sub>3</sub>: experiments and crystallite-scale modeling, *Chem. Eng. J.* 230 (2013) 584–594.